(1)

AD-A224 823

CHARACTERIZATION OF MCT (MERCURY CADMIUM TELLURIDE) BY EER (ELECTROLYTE ELECTROREFLECTANCE)

BY

Unchul Lee
B.S. Seoul National University
M.S. University of Illinois at Chicago

THESIS

Submitted in partial fulfillment of the requirements
for the degree of Doctor of Philosophy in Physics
in the Graduate College of the
University of Illinois at Chicago, 1985

Chicago, Illinois
Department of Physics

DEDICATION

FOR MY FAMILY, ESPECIALLY SUNYOUNG

ACKNOWLEDGEMENTS

I want to take this opportunity to thank Dr. Paul M. Raccah, my advisor, for his encouragements and guidances to finish my research. Otherwise it would not have been possible for me to reach my goal, the Ph. D.

Also many thanks to Dr. James W. Garland for his theoretical insights and to Dr. L. L. Abels for his experimental helps and to Dr. Lambert Schoonveld for his helps with the computer.

I also want to thank the electronic shop staffs and machine shop staffs as well as department staffs for their enormous helps.

It is appropriate at this time to give a words of thanks to my parents and aunt for their emotional support. Special thanks are due my aunt who put me through school all the way from high school to the college allowing me to come to U.S.A. to seek the Ph. D.

Most of all I have to thank my wife Sunyoung who put up with my study for these many years. Her support and devotion have made it possible to weather many rough times until this moment.

ABSTRACT

In Chapter I, a brief discussion of the development and significance of modulation spectroscopy is given.

In the following Chapters(II - V) the theoretical explanation of Electroreflectance spectroscopy and the connection between the lineshape and the interband energy transition are discussed.

Chapter VI is assigned for the experimental setup and data gathering procedures.

Chapters VII and VIII contain the main body of my research where the characterization of MCT and the modified theory of electroreflectance are discussed in detail and sample fitting for modified theory is shown.

In Chapter IX the evidence for the change in the type of MCT is explained as resulting from stress. Chapter X is reserved for summary of the thesis.

CONTENTS

Chapter I

INTRODUCTION

The lines observed in the absorption and emission spectra of nearly isolated atoms and ions are extremely sharp. As a result, their wavelengths can be determined with great accuracy. The large amount of extremely precise spectroscopic data for atoms and ions accumulated during the last century and the early part of the this century has been responsible for the initial development and many subsequent refinements of quantum theory. Molecular spectra, while usually less sharper than atomic spectra are also sharp. Positions of spectral lines can be determined with enough accuracy to check quantum mechanical calculations of the electronic structure of the molecules. By the same token one concludes that a study and understanding of the optical properties of solids would contribute to the knowledge of their electronic structure.

However it turns out that due to the high density of solids broad spectra result which provide less help in understanding the electronic structure of the solids. In other words the spectra of reflectance for a solid are broad and the structures of reflectance spectra are not sharp. Besides accurate reflectivity measurements are somewhat difficult when you want to scan long wavelength ranges. Seraphin's original work (1964) on electroreflectance in germanium, opened a wide field of possibilities for studying optical structure. Fig. (1) (Aspnes, 1980).

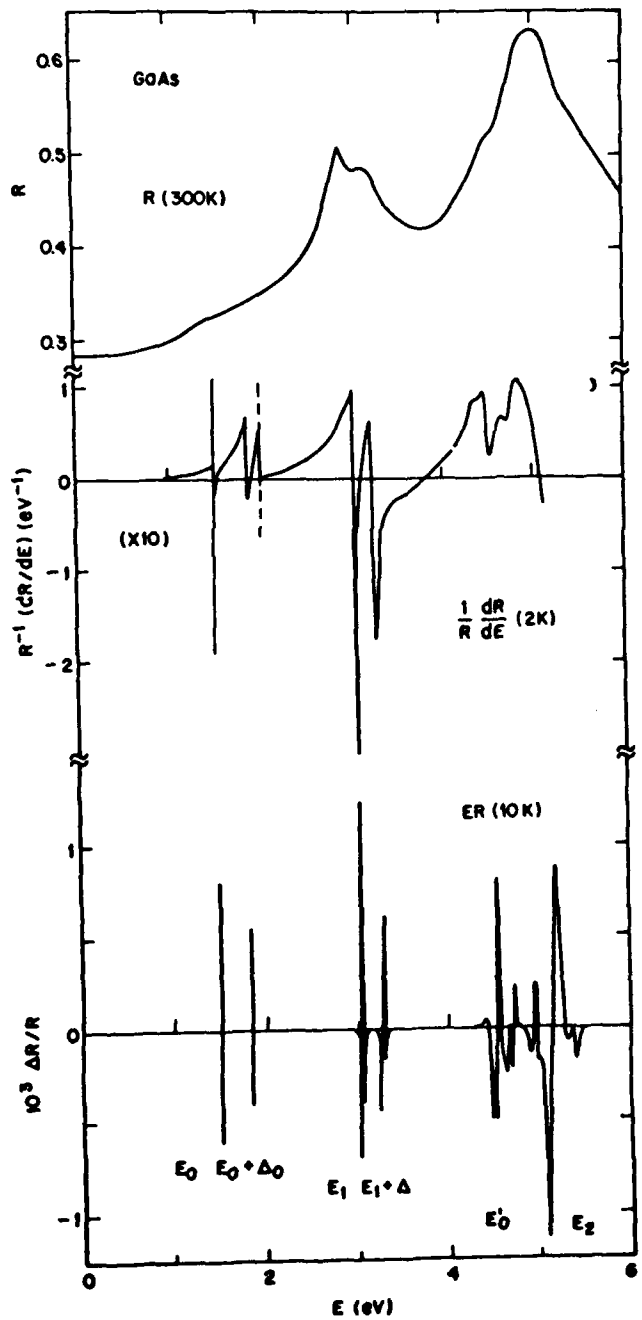

Fig. 1. A comparison of three types of spectra from 0–6 eV for a typical semiconductor, GaAs. Top: reflectance R (Philipp and Ehrenreich 1963); middle: energy-derivative reflectance (Sell and Stokowski 1970); bottom: low-field electroreflectance (Aspnes and Studna 1973).

Table I
Characteristics of some commonly used modulation techniques.

Technique	Nature	Type	Variable	Sample parameters affected	Lineshape type
Wavelength modulation energy derivative reflectance	Internal	Scalar	Wavelength λ: energy $\hbar\omega$	-	1st derivative
Spectroscopic ellipsometry	Internal	Scalar	Wavelength λ: energy $\hbar\omega$	-	Absolute
Composition modulation	Internal	Scalar	Sample compared to control sample	-	Complicated
Thermomodulation	External	Scalar	Temperature T	Thresholds E_g Broadening parameters Γ	1st derivative
Hydrostatic pressure	External	Scalar	Pressure P	Thresholds E_g	1st derivative
Light modulation (Photoreflectance) (Photovoltage)	External	Scalar or tensor	Intensity I of secondary beam	Carrier concentration or surface electric field	Complicated
Uniaxial stress	External	Tensor	Stress X	Thresholds E_g Matrix elements	1st derivative
Electric field	External	Tensor	Field E	Electron energy $E(k)$	3rd derivative (low) Franz-Keldysh oscillations (high)
Magnetic field	External	Tensor	Field H	Electron energy levels	Landau levels

Technique references

1. Sell (1970)
2. Shaklee and Rowe (1970)
3. Shen (1973)
4. Azzam and Bashara (1977)
5. Aspnes and Hauge (1976)
6. McNatt and Handler (1969)
7. Holbrook and Hummel (1973)
8. Batz (1972)
9. Martinez (1979)
10. Wang et al. (1967)
11. Sell (1973)
12. Cardona (1969)
13. Balslev (1972)
14. Electrolyte: Cardona et al. (1967)
15. MOS: Fischer (1971)
16. Schottky barrier: Studna (1975)
17. Transverse: Rehn (1973), Forman et al. (1970)
18. Electroabsorption: Frova and Handler (1965)
19. Aggarwal (1972)
20. Hensel and Suzuki (1974)

Table I
(*continued*)

Principal sample parameters measured	Principal advantages	Applicability	Disadvantages	Techn. refs.	Theory refs.
E_g, Γ	Universal applicability Minimal sample preparation. Fast, convenient	Any material	Measurement system can generate intrinsic structure not easy to eliminate	1, 2, 3	1, 2
Dielectric function	As energy derivative reflectance but on ϵ_1, ϵ_2 directly	Any material	Strongly influenced by surface preparation and thin films	4, 5	3
Doping, alloying effects	Obtains differences for parameters impossible to vary cyclically	Any material	Two samples/beam motion involved; alignment and surface preparation critical	6, 7	4
E_g, Γ dE_g/dT $d\Gamma/dT$	Wide applicability; identifies Fermi level transitions in metals	Any material	Slow response (1–40 Hz) Broad spectra	8	5, 6, 7
Deformation potentials		Any material	Cannot be modulated; must be used in conjunction with another technique	9	8
E_g	Convenient; minimal sample preparation required	Any material	Effect on material usually not well defined	10	9
E_g, Γ Symmetries Deformation potentials	Symmetry determination	"Hard" materials	Difficult to modulate Limited to high fracture/yield stress materials	11, 12, 13	10, 11, 12, 13
E_g, Γ Effective masses Symmetries Impurity concentrations	Very high resolution. Only high-resolution technique usable in vuv	Semiconductors and insulators	Requires certain resistivity ranges	14, 15, 16, 17, 18	14, 15, 16, 17
E_g, effective masses	Extremely high resolution	Any material	Advantages realized only for lower conduction band minima	19, 20	18, 19

Theory references

1. Cardona (1969)
2. Batz (1972)
3. Azzam and Bashara (1977)
4. Holbrook and Hummel (1973)
5. Cardona (1969)
6. Batz (1972)
7. Cohen (1979)
8. Martinez (1979)
9. Cardona (1970)
10. Kane (1968)
11. Cardona (1969)
12. Pollak (1973)
13. Balslev (1972)
14. Low fields: Aspnes and Studna (1973)
15. High field: Aspnes et al. (1968)
16. Symmetry: Bottka and Fischer (1971)
17. Electroabsorption: Blossey and Handler (1972)
18. Aggarwal (1972)
19. Suzuki and Hensel (1974)

It became clear as a result of this work that fairly sharp structure could be obtained by measuring the derivative of R with respect to some external parameter, such as applied electric field instead of the reflectivity R. This technique modulates the reflectance of a sample either through a periodic change of such external parameters as electric field, pressure, or temperature (external modulation), or through the change of such measuring system parameters as wavelength (internal modulation). Table(1) (modulation techniques) (Aspnes, 1980). Since the signal for modulation spectroscopy is small phase sensitive detector is required, a fact that delayed modulation spectroscopy until the full-fleged development of electronics.

The phase sensitive detection technique allowed experimentalists to observe small changes in the optical properties of crystals induced by electric fields and other perturbations. Band structure calculations (wnich were also at developing stages at that time) indicated the possibility of associating these small changes with perturbation-induced effects at specific points in the Brillouin zone. As a result, it was thought that modulation spectroscopy could be used to probe the energy band structures of crystals.

At first reflectivity experimemts were used to test or verify the predictions of band structure calculations of the interband transition energies at critical points of the Brillouin zone. However it became increasingly clear that a higher resolution experimental method was desirable. Following the pioneering work of Seraphin(1964) and of Cardona(1969), the explosive development of modulation spectroscopy, coupled with rapid advances in band-structure calculational techniques, assured

rapid progress in the understanding of the electronic properties of semiconductor crystals.

The primary methods of modulation spectroscopy have been electroreflectance, photoreflectance, piezoreflectance, thermoreflectance and wavelength modulation. Because it yields the sharpest spectra of any modulation techniques, electroreflectance (ER) has been and still is the most widely used technique, particularly in its remarkably simple low-field electrolyte electroreflectance (EER) version. The extensive experimental and theoretical work of Aspnes and coworkers has played a cental role in the understanding of the physics of ER. Following the Franz-Keldysh(1958) approach Aspnes has provided the most lucid and comprehensive study of the effects of an applied electric field on the optical properties of a perfect crystal. Assuming that the only significant effects of the electric field are to break the translational symmetry of the unperturbed crystal and to accelerate the electron-hole pair produced by the absorption of a photon, he found theoretically(1973) that in the low field regime the difference between the dielectric function of a crystal submitted to an electric field and the unperturbed dielectric function is proportional to the third derivative with respect to energy of a linear combination of the real and imaginary parts, ϵ_1 and ϵ_2, of the unperturbed dielectric function $\epsilon(E)$ and is proportional to the square of the electric field.

Because ϵ_1 and ϵ_2 can be measured by automatic spectroscopic ellipsometry(ASE), it is possible to check this theory by computing numerically from ASE data the third-derivative lineshape (TDL) which, according to

the theory, should be proportional to the ER spectrum. For relatively defect-free surfaces of centrosymmetric semiconductors, the experimental ER spectrum has been found to be quadratic in $\bar{E}_m$ to be proportional to the TDL obtained from ASE data, verifying the predictions of the theory.

Aspnes also derived (1973) within the parabolic-band approximation a functional representation for the ER signal which yields remarkably good fits to all low-field ER spectra obtained from high-quality centrosymmetric crystals. That representation has been extremely useful because no single feature in an ER spectrum can be unambiguously related to a critical-point interband transition energy, E_i. Thus, in order to obtain an accurate value for E_i one must fit the entire experimental spectrum in the vicinity of E_i to a parametrized theoretical lineshape of which E_i is only one of the parameters.

With time, interest in the properties of the ternary and quaternary semiconducting alloys has been increased greatly, and the relationship between the alloy composition x and the values of the transition energies E_i has received considerable attention, primarily for experimental reason. In the absence of phase transitions, immiscibility regions and direct-gap/indirect-gap transitions the E_i can be represented rather accurately by quadratic expressions of the form $E_i = a + bx + cx^2$. Such a simple relationship permits one to compute easily the alloy composition x as a function of the experimentally determined value of E_i. In addition, by etching in controlled steps it is possible to profile the alloy composition of an epitaxial layer with a high depth resolution since the choice of a convenient interband transition, such

as E_1, which is in the visible, assures that for most semiconductors the light penetration will be no greater than 300 to 600 Å.

The parameters for quadratic relationship between alloy composition x and interband transition energy E_i have been determined numerous times for MCT. But the published values do not agree one another. Therefore establishing good parameter values for the quadratic eqution is one of my most important contributions to profile MCT. Another job is calibration of etching rate for MCT by Br/Met.

Electrolyte electroreflectance has also proven to be very useful as a characterization technique in assessing the quality of semiconductor alloys grown either in the bulk or by epitaxy. However, the systematic use of lineshape fitting rapidly showed that for samples rich in defects the lineshape was unusually broad and that in such cases the functional form derived by Aspnes(1973) could be fit satisfactorily to the EER data only close to a critical point energy. This observation coincided with the observation of discrepancies between the linewidth measured by fitting the EER data and that measured by fitting the numerical third derivative of the dielectric function obtained by ASE. These discrepancies contradicted the fundamental result of Aspnes that the EER signal should be proportional to the third derivative of a linear combination of the real and imaginary parts of the dielectric function. Thus, they led us to reconsider the theory of ER and, in particular, to generalize the theory in such a manner as to take into account the effects of the coupling of the modulating electric field to defects. The generalized theory has terms which are proportional to first and second derivatives

of $\epsilon(E)$ as well as the usual third derivative term found by Aspnes. The amplitudes of these new terms were found to be approximately proportional to the density of extended defects and the density of point defects, respectively. The use of the new theory in fitting the data yields a measure of the relative densities of different types of defects in different samples.

By coupling photoemission with EER studies it was possible to analyze the response of MCT to mechanical shock, and conclude that under the stress, mercury tends to migrate, at least in part, via charged defects conferring an n character to the material.

Chapter II

ELECTROREFLECTANCE (ER)

Electroreflectance (Electric field modulation) has become the most popular of all modulation techniques, due to the simplicity of the EcR (Electrolyte Electroreflectance) which is also the method employed in this work. The theoretical groundwork for this type of modulation was done by Franz and Keldysh (1958) (hence the name Franz-Keldysh effect) and extended by Callaway (1963, 1964), Tharmalingam (1963) and Aspnes (1968).

2.1 PHENOMENOLOGICAL DESCRIPTION OF ELECTROREFLECTANCE (ER)

The relative modulation $\Delta R/R$ (ΔR is a modulated reflectance) impressed onto the reflected beam of intensity R is the basic quantity measured in electroreflectance. Before we try to connect $\Delta R/R$ with ϵ_1 (real part of the dielectric function) and ϵ_2 (imaginary part of the dielectric function) we must make an assumption about the manner in which the modulation parameter affects the sample. In the most simple case, we can assume that the modulation induces a homogeneous change in the optical constants ϵ_1 and ϵ_2. The reflecting surface is then a discontinuous interface between two media that are homogeneous throughout at given time. Piezoreflectance (uniaxial stress modulation) and thermoreflectance (heat pulse modulation) can probably be treated in this manner.

In electroreflectance, the situation can be more complicated. The ratio of field penetration to light penetration governs the use of either of two different approaches. If the light penetrates little compared to the electric field, we can consider the medium homogeneously affected. If, however, the light penetrates much further than the electric field, it encounters a medium of variable optical properties on its way in and out of the surface.

2.2 NORMAL INCIDENCE AT THE INTERFACE

The reflectance for light impinging at normal incidence onto an ideal solid surface can be derived simply from a consideration of the boundary conditions for $\bar{E}$ and $\bar{H}$ at the interface. At the interface we can write

$$E_i + E_r = E_t \tag{1}$$

where subscript i, r and t represent respectively, the incident, reflected and transmitted waves at the interface. Similar equations hold for H, but with a change in sign for H_r.

$$H_i - H_r = H_t. \tag{2}$$

In the vacuum, E = H, whereas in the medium, $\hat{n}$ is a complex refractive index,

$$H = (\hat{n}/\mu^{\frac{1}{2}})E. \tag{3}$$

Therefore when we use Eq. (3) Eq. (2) becomes

$$E_i - E_r = \hat{n}E_t \tag{4}$$

where the permeability μ has been taken as a unity. Eqs. (1) and (4) are easily solved to yield a reflectance wave amplitude

$$\hat{r} = E_r/E_i = (1 - \hat{n})/(1 + \hat{n}) \ . \tag{5}$$

The reflectivity is then given by

$$R = \hat{r}^*\hat{r} = |(1 - \hat{n})/(1 + \hat{n})|^2 = [(1 - n)^2 + \kappa^2]/[(1 + n)^2 + \kappa^2] . \tag{6}$$

From the relation $\epsilon = \epsilon_1 + i\epsilon_2 = (n + i\kappa)^2$ for the nonmagnetic materials,

$$\epsilon_1 = n^2 - \kappa^2 \tag{7}$$

$$\epsilon_2 = 2n\kappa \ . \tag{8}$$

If we solve Eqs. (7) and (8) for n and κ we get

$$n = \{1/2[(\epsilon_1^2 + \epsilon_2^2)^{\frac{1}{2}} + \epsilon_1]\}^{\frac{1}{2}} \tag{9}$$

$$\kappa = \{1/2[(\epsilon_1^2 + \epsilon_2^2)^{\frac{1}{2}} - \epsilon_1]\}^{\frac{1}{2}} . \tag{10}$$

2.3 HOMOGENEOUS MODULATION OF THE REFLECTING MEDIUM

We assume here that the dielectric function $\epsilon = \epsilon_1 + i\epsilon_2$ of the reflecting material is uniformly changed by the modulation by the amounts $\Delta\epsilon_1$ and $\Delta\epsilon_2$.

The reflecting surface then establishes a discontinuous interface between two different but homogeneous media for which Fresnel's reflection equation applies. For normal incidence of light, it has the form

$$R = [(\epsilon_1^2 + \epsilon_2^2)^{\frac{1}{2}} - (2\epsilon_1 + 2(\epsilon_1^2 + \epsilon_2^2)^{\frac{1}{2}})^{\frac{1}{2}} + 1] \quad (11)$$

$$/[(\epsilon_1^2 + \epsilon_2^2)^{\frac{1}{2}} + (2\epsilon_1 + 2(\epsilon_1^2 + \epsilon_2^2)^{\frac{1}{2}})^{\frac{1}{2}} + 1].$$

Its total differential with respect to ϵ_1 and ϵ_2 provides a phenomenological description of the reflectance modulation.

$$\Delta R/R = \alpha(\epsilon_1, \epsilon_2)\Delta\epsilon_1 + \beta(\epsilon_1, \epsilon_2)\Delta\epsilon_2 \quad (12)$$

where

$$\alpha = 2\gamma/(\gamma^2 + \delta^2) \quad (13)$$

$$\beta = 2\delta/(\gamma^2 + \delta^2) \quad (14)$$

$$\gamma = n(n^2 - 3\kappa^2 - n_o)/n_o \quad (15)$$

$$\delta = \kappa(3n^2 - \kappa^2 - n_o)/n_o \quad (16)$$

where n_0 is the refractive index of the nonabsorbing medium of incidence and κ satisfies the relation $\epsilon^{\frac{1}{2}} = n + i\kappa$.

2.4 INHOMOGENEOUS MODULATION OF THE REFLECTING MEDIUM

For electroreflectance where the spatial variation of electric field over the penetration depth of the light can be considerable the changes of dielectric constants due to the electric perturbation cannot be assumed to be homogeneous always.

We assume a semi-infinite dielectric $-\infty < z < z_s$ (subscript s stands for surface) in which the dielectric function $\epsilon = \epsilon_1 + i\epsilon_2$ is perturbed by a z-dependent change $\Delta\epsilon(z) = \Delta\epsilon_1(z) + i\Delta\epsilon_2(z)$ that is small and disappears at large distances into the medium so that $|\Delta\epsilon(z)| < |\epsilon|$ and $\lim_{z\to-\infty}|\Delta\epsilon(z)| = 0$. The effect of $\Delta\epsilon(z)$ upon wave propagation of an electric field of magnitude $\tilde{E}$ in the dielectric can be approximated by a trial solution

$$\tilde{E}(z) = \tilde{E}_o \exp[i\{-Kz + \phi(z)\}] \tag{17}$$

of the wave equation, where $\phi(z)$ is a complex z-dependent phase and K is the unperturbed propagation constant.

Neglecting terms of second order in $\Delta\epsilon(z)/\epsilon$, the relative change in reflectance can be written (ϕ' is the derivative of ϕ) as

$$\Delta R/R = \{R(\phi') - R(0)\}/R(0) = \alpha\langle\Delta\epsilon_1\rangle + \beta\langle\Delta\epsilon_2\rangle, \tag{18}$$

where

$$\langle \Delta\epsilon \rangle = \langle \Delta\epsilon_1 \rangle + i\langle \Delta\epsilon_2 \rangle = -2iKe^{2iKz_s} \int_{-\infty}^{z_s} dz' e^{-2iKz'} \Delta\epsilon(z') \qquad (19)$$

where α and β are the fractional coefficients defined in Eqs. (13) and (14). In Eq. (19) the frequency dependence of $\Delta\epsilon(z')$ is independent of z' so that the whole effect of an inhomogeneous electric field is just to multiply $\Delta\epsilon(z=0)$ by a complex constant.

Chapter III

THEORETICAL CONCEPTS IN ER

The rich trace of structures in $\Delta R/R$ compared with reflectance R can be explained theoretically following the theory developed by Aspnes et al(1972a,b). The effect of a uniform field on the electron-dependent properties of a crystalline solid is described in the one-electron approximation by the solution to the time-dependent Schrödinger equation

$$[H_o + e\bar{E}.\bar{r}]\Psi(\bar{r},t) = i\hbar\partial\Psi(\bar{r},t)/(\partial t) \qquad (20)$$

where H_o is the unperturbed Hamiltonian defined as $H_o(\bar{r}) = (-\hbar^2/(2m))\nabla^2_{\bar{r}} + V(\bar{r})$, $\Psi(\bar{r},t)$ is the one-electron wave function of the system, and $\bar{E}$ is the constant electric field.

3.1 INTERACTION OF LIGHT WITH MATTER

In order to link the theory to experiment we first consider the interaction of light with matter. There are several different formalisms which may be used to describe this interaction in terms of the properties of the wave function of a solid, for example the standard perturbation theory approach used by Seitz or Pines, the Kubo formalism or various Green's function techniques. We outline here the perturba-

tion theory approach, which has been used predominently in the calculation of electric field effects.

As usual, the medium is assumed to be infinite, isotropic and homogeneous. An electromagnetic wave propagating in this medium can be described by its field $\bar{E}(\bar{r},t)$ or its vector potential $\bar{A}(\bar{r},t)$. These quantities are related by the equation $\bar{E}(\bar{r},t) = (-1/c)(\partial/\partial t)\bar{A}(\bar{r},t)$ in the Coulomb gage. Since the wavelength of the propagating wave is much larger than the atomic dimensions of the system, it is reasonable to use macroscopic forms of Maxwell's equations.

For an electrically neutral solid with no external current flow, the Fourier transforms of $\bar{D}(\bar{r},t)$ (the electric displacement), the applied electric field $\bar{E}(\bar{r},t)$, current density $\bar{J}(\bar{r},t)$, and polarization $\bar{P}(\bar{r},t)$ are related (by definition) as

$$\bar{\bar{D}}(\bar{k},\omega) = \bar{\bar{E}}(\bar{k},\omega) + 4\pi\bar{\bar{P}}(\bar{k},\omega) \tag{21}$$

$$= \bar{\bar{E}}(\bar{k},\omega) + (i4\pi/\omega)\bar{\bar{J}}(\bar{k},\omega).$$

For sufficiently weak fields, the current term $\bar{J}(\bar{k},\omega)$ will depend linearly on $\bar{E}(\bar{k},\omega)$ in the random-phase approximation and Eq. (21) can be written (in the linear optical and random-phase approximation) as

$$\bar{\bar{D}}(\bar{k},\omega) = \bar{\bar{\epsilon}}(\bar{k},\omega).\bar{\bar{E}}(\bar{k},\omega). \tag{22}$$

The tensor $\bar{\epsilon}(\bar{k},\omega)$ relating $\bar{D}$ and $\bar{E}$ in Eq. (22) is defined to be the dielectric function. The importance of the dielectric function is that it completely describes wave propagation in the medium on the macroscopic

scale. By matching the boundary conditions among incident, reflected, and transmitted wave at an interface of the medium with another, the reflectance R and transmittance T may be expressed in terms of it. The properties of the solid enter through the source term $(4\pi i/\omega)\bar{J}(\bar{k}, \omega)$ in Eq. (21), and $\bar{\epsilon}(\bar{k},\omega)$ is calculated by evaluating the Fourier transform of the spectral average of the microscopic current operator $\bar{J}(\bar{r},t)$ to terms linear in the electromagnetic wave perturbation $\bar{A}(\bar{r},t)$ or $\bar{E}(\bar{r},t)$, using the wave functions of the system. The microscopic current operator is (- e) times the probability current density of quantum mechanics, or

$$\bar{J}(\bar{r},t) = (ie\hbar/(2m))(\Psi^*\nabla\Psi - \Psi\nabla\Psi^*) - (e^2\bar{A}/(mc))\Psi^*\Psi \qquad (23)$$

where $\Psi = \Psi(\bar{q},\bar{r},t)$ represents a one-electron state of quantum number $\bar{q}$ which is a solution of the perturbed Schrödinger equation

$$[1/(2m)(\bar{p} + e\bar{A}(\bar{r},t)/c)^2 + V(\bar{r},t)]\Psi(\bar{q},\bar{r},t) = i\hbar(\partial/(\partial t))\Psi(\bar{q},\bar{r},t) \qquad (24)$$

Although other vector potentials may be included in the Hamiltonian operator of Eq. (24), we show explicitly only the vector potential of the (real) traveling wave

$$\bar{A}(\bar{r},t) = \hat{e}A_o\cos(\bar{k}.\bar{r} - \omega t) \qquad (25)$$

with polarization vector $\hat{e} \perp \bar{k}$. In the linear optical approximation, only terms to first order in $\bar{A}$ are kept and the wave function $\Psi(\bar{q},\bar{r},t)$ may be calculated to first order in $\bar{A}$ in terms of the complete set of

eigenfunctions $\Psi_0(\bar{q},\bar{r},t)$ of Eq. (24) with $\bar{A} = 0$. The dipole approximation where the spatial dependence of $\bar{A}$ is neglected is used.

If the eigenstate $\Psi_0(\bar{q},\bar{r},t)$ represents a stationary state of a time-independent Hamiltonian, the time dependence can be separable and the dielectric function may be easily evaluated in general form. The first-order corrections linear in $\bar{A}$ are calculated for the wave functions $\Psi_0(\bar{q},\bar{r},t)$ by standard time-dependent perturbation theory. The current operator is evaluated with these wave functions to terms linear in $\bar{A}$. By taking the Fourier transform of the resulting expression and using Eqs. (21) and (22), we have the expression (for an isotropic crystal)

$$\epsilon(\omega) = \epsilon_1(\omega) + i\epsilon_2(\omega) \tag{26}$$

$$= 1 - 4\pi e^2/(m\omega^2 V)\Sigma_{\bar{q}}\langle N(\bar{q})\rangle + 4\pi e^2/(m^2\omega^2\hbar V)\Sigma_{\bar{q}\bar{q}'}|\hat{e}\cdot\bar{P}_{\bar{q}\bar{q}'}|^2$$

$$\times \langle N(\bar{q})\rangle[1 - N(\bar{q}')]\{2P\omega_{\bar{q}'\bar{q}}/(\omega_{\bar{q}'\bar{q}} - \omega) + i\pi[\delta(\omega_{\bar{q}'\bar{q}} - \omega)$$

$$- \delta(\omega_{\bar{q}'\bar{q}} + \omega)]\},$$

where $\epsilon_1(\omega)$ and $\epsilon_2(\omega)$ are the real and imaginary parts of $\epsilon(\omega)$, V is the crystal volume, $\hbar\omega_{\bar{q}'\bar{q}}$ represents the energy difference between the states $\bar{q}'$ and $\bar{q}$

$$E_{\bar{q}'\bar{q}} = \hbar\omega_{\bar{q}'\bar{q}} = E_{\bar{q}'} - E_{\bar{q}}, \tag{27}$$

where $\bar{P}_{\bar{q}'\bar{q}}$ is the momentum matrix element taken between constant energy states,

$$\bar{P}_{\bar{q}'\bar{q}} = \langle\Psi(\bar{q}',\bar{r})\,|\,(\hbar/i)\nabla_{\bar{r}}\,|\Psi(\bar{q},\bar{r})\rangle, \tag{28}$$

P means the principal value, and $\langle N(\bar{q})\rangle$ represents the occupation probability of the state $\bar{q}$

$$\langle N(\bar{q})\rangle = [1 + \exp((E_{\bar{q}} - E_F)/(kT))]^{-1} \tag{29}$$

where E_F is Fermi energy and $\langle N(\bar{q})\rangle$ describes the Pauli exclusion principle and must be added as an ad hoc correction.

It is convenient to separate the real part $\epsilon_1(\omega)$ into the Kramers-Kronig transform of the imaginary part and a remainder proportional to ω^{-2}, which gives the interband contribution to the plasma term. Since

$$\omega^{-2}(\omega_{\bar{q}',\bar{q}})(\omega^2_{\bar{q}',q} - \omega^2)^{-1} = [(\omega_{\bar{q}',\bar{q}})(\omega^2_{\bar{q}',q} - \omega^2)]^{-1} + (\omega_{\bar{q}',\bar{q}}\omega^2)^{-1} \tag{30}$$

Eq. (26) can be written as

$$\epsilon(\omega) = 1 - \omega_p^2/\omega^2 + (4\pi e^2)/(m^2\hbar V)\,\Sigma_{\bar{q}',\bar{q}}|\hat{e}.\bar{P}_{\bar{q}',\bar{q}}|^2\langle N(\bar{q})\rangle[1 - \langle N(\bar{q}')\rangle] \times \{2P[\omega_{\bar{q}',\bar{q}}(\omega^2_{\bar{q}',q} - \omega^2)]^{-1} + i\pi/\omega^2[\delta(\omega_{\bar{q}',\bar{q}} - \omega) - \delta(\omega_{\bar{q}',\bar{q}} + \omega)]\}, \tag{31}$$

where the plasma frequency is given by

$$\omega_p^2 = ((4\pi e^2)/(mV))\,\Sigma_{\bar{q}}\langle N(\bar{q})\rangle\{1 - \Sigma_{\bar{q}',2}[|\hat{e}.\bar{P}_{\bar{q}',\bar{q}}|^2(1 - \langle N(\bar{q}')\rangle)]/m\hbar\omega_{\bar{q}',\bar{q}})\}. \tag{32}$$

As an example, the dielectric function of an insulator in which the constant energy eigenfunctions are of Bloch form is given by

$$\epsilon_1(\omega) + i\epsilon_2(\omega) = 1 + 4\pi e^2/(m^2\hbar)\,((2/(2\pi)^3)\Sigma\int_{BZ} d^3k\,|\hat{e}.\bar{P}_{n'n}(\bar{k})|^2 \quad (33)$$

$$\times\ \{2P[(\omega_{n'n}(\bar{k}))\,(\omega^2_{n'n}(\bar{k}) - \omega^2)]^{-1}$$

$$+\ i\pi/(\omega^2)\,[\delta(\omega_{n'n}(\bar{k}) - \omega) - \delta(\omega_{n'n}(\bar{k}) + \omega)]\}$$

where the quantum numbers $\bar{q}$ are now the wave numbers $\bar{k}$ and band indices n, $\bar{P}_{n'n}(\bar{k})$ is the matrix defined as

$$\int_V d^3r\,\phi^*_{n'}(\bar{k},\bar{r})\,\bar{P}\,\phi_n(\bar{k},\bar{r}) = \delta_{k'k}\bar{P}_{n'n}(\bar{k}) \quad (34)$$

where $\bar{p} = (\hbar/i)\nabla$, $\phi_n(\bar{k},\bar{r}) = \exp(i\bar{k}.\bar{r})\,u_n(\bar{k},\bar{r})$ (Bloch function) and

$$\bar{P}_{n'n}(\bar{k}) = N\int_\Omega d^3r\,U^*_{n'}(\bar{k},\bar{r})\,\bar{p}\,U_n(\bar{k},\bar{r}) \quad (35)$$

where $N = V/\Omega$, Ω = unit cell volume.

$$E_{n'n}(\bar{k}) = \hbar\omega_{n'n}(\bar{k}) = E_{n'}(\bar{k}) - E_n(\bar{k}) \quad (36)$$

is the interband energy separation, the sum of $\bar{k}$ over the Brillouin zone has been replaced with an integral as

$$\Sigma_k \rightarrow [V/(2\pi)^3]\int_{BZ} d^3k \quad (37)$$

and a factor of 2 has been included for spin degeneracy. The bands are assumed to be either completely filled or empty, so $\omega_p = 0$.

We now indicate the connection of the dielectric function to experiment. Since the dielectric function determines the propagation of an electromagnetic wave in a medium, it determines the energy loss per unit length, and also the reflectivity by imposing boundary conditions on the surface. The solution of the one dimensional Maxwell equation for a monochromatic transverse wave,

$$[\nabla^2_{\bar{r}} + (\omega/c)^2 \epsilon(\omega)]\bar{E}(\bar{r},t) = 0, \tag{38}$$

where $\bar{E}(\bar{r},t) = \hat{e}E_0 \exp(i\bar{k}.\bar{r} - i\omega t)$ gives the relation between $\epsilon(\omega)$ and the complex propagation vector $\bar{k}$ of the wave in the solid

$$(c/\omega)|\bar{k}| = [\epsilon(\omega)]^{\frac{1}{2}} = n(\omega) + i\kappa(\omega). \tag{39}$$

Equation (39) defines the refraction and absorption indices n and κ, respectively. Calculation of Poynting vector gives the attenuation in terms of the absorption coefficient

$$\alpha = \omega\epsilon_2(\omega)/(nc). \tag{40}$$

In modulation experiments changes are induced in the dielectric function (we take the perturbation to be a function of an external electric field $\bar{E}$),

$$\Delta\epsilon(\omega,\bar{E}) = \epsilon(\omega,\bar{E}) - \epsilon(\omega,0) = \Delta\epsilon_1(\omega,\bar{E}) + i\Delta\epsilon_2(\omega,\bar{E}) \tag{41}$$

therefore changes are also induced in the reflectance and absorption and can be described by the equation

$$\Delta R(\omega,\bar{E})/R = \alpha(\omega)\Delta\epsilon_1(\omega,\bar{E}) + \beta(\omega)\Delta\epsilon_2(\omega,\bar{E}). \tag{42}$$

3.2 CRITICAL POINT

The dielectric function of a periodic crystal exhibits features that are due to the topological properties of the continuous, periodic eigenvalues $E_n(\bar{k})$ which describe the energy of an electron in the Bloch state $\phi_n(\bar{k},\bar{r})$. These appear most clearly in ϵ_2 where the δ function causes singularities at certain points in the Brillouin zone, so called "critical points," where the gradient of the interband energy vanishes (i.e. the constant-energy surfaces are parallel). The mathematical expression is

$$\nabla_{\bar{k}}(E_{n'} - E_n) = 0. \tag{43}$$

A vanishing of the interband gradient can occur in four topologically distinct ways between two nondegenerate bands: at a maximum, at a minimum, or at either of two types of saddle points. These singularities are extremely important from an experimental point of view, since the dominent perturbation-induced changes in the dielectric function occur in the vicinity of these points. To show these singularities explicitly, we transform the imaginary part of Eq. (33) associated with $\delta[\omega_{n',n}(\bar{k}) - \omega]$ from a volume integration in $\bar{k}$ space to a surface integration using the coordinate transformation

$$d^3k = dE dS_{n'n} / |\nabla_{\bar{k}} E_{n'n}(\bar{k})| \tag{44}$$

where $dS_{n'n}$ represents an element of area of the constant interband energy surface $E_{n'n}(\bar{k}) = E$ in $\bar{k}$ space, and dE is the energy increment in that space. The result is

$$\epsilon_2(\omega) = (2\pi e/m\omega)^2 \Sigma_{n'n} [2/(2\pi)^3] \int_S dS_{n'n} \int_{En'n} dE \, |\hat{e}.\bar{P}_{n'n}(\bar{k})|^2 \tag{45}$$

$$/|\nabla_{\bar{k}} E_{n'n}(\bar{k})| \times \delta(E_{n'n} - \hbar\omega).$$

Using the properties of the δ function and assuming the momentum matrix element to vary slowly with $\bar{k}$, we obtain

$$\epsilon_2(\omega) = (2\pi e/m\omega)^2 \Sigma_{n'n} |\hat{e}.\bar{P}_{n'n}|^2 J_{n'n}(\omega) \tag{46}$$

where

$$J_{n'n}(\omega) = 2/(2\pi)^3 \int_S dS/|\nabla_{\bar{k}}[E_{n'}(\bar{k}) - E_n(\bar{k})]|_{En'n=\hbar\omega} \tag{47}$$

is the joint density-of-states for interband transitions. The singularities of critical points in ϵ_2 or in the joint density-of-states are now evident: they occur where the gradient of interband energy vanishes, i.e., when $\nabla_k[E_{n'}(\bar{k}) - E_n(\bar{k})] = 0$. The four types of nondegenerate critical points can be explicitly shown by expanding the interband energy as a function of wave vector about the critical points $\bar{k}_c$ in a power series

$$E_{n'n}(\bar{k}) = E_{n'n}(\bar{k}_c) + 1/2 \Sigma_{ij} \partial^2 E_{n'n}/\partial k_i \partial k_j |_{\bar{k}=\bar{k}_c} (k - k_c)_i (k - k_c)_j \tag{48}$$

where summation indices i, j represent the coordinate axes x, y, z. Since the gradient vanishes at the critical point itself, an expansion about this point has no terms linear in wave number, and only the constant and quadratic terms appear in the parabolic approximation. In the language of analytic geometry, Eq.(48) describes a constant energy surface in the vicinity of $\bar{k}_c$. The expansion coefficients can be rewritten in the coordinate system which diagonalizes Eq.(48),

$$E_{n'n}(\bar{k}) = E_{n'n}(\bar{k}_c) + \hbar^2/2[(k_x - k_{xc})^2/\mu_x + (k_y - k_{yc})^2/\mu_y + (k_z - k_{zc})^2/\mu_z] \quad (49)$$

where we define the reduced mass μ_i as

$$1/\mu_i = 1/m^*_{ei} + 1/m^*_{hi} = 1/\hbar^2\partial^2 E_{n'}/\partial k_i^2 - 1/\hbar^2\partial^2 E_n/\partial k_i^2, \quad i=x,y,z, \quad (50)$$

and where m_e^* and m_h^* are the effective masses of the electron and hole, respectively. A positive reduced mass thus corresponds to a minimum in energy along that particular direction, and a negative mass corresponds to a maximum.

Since there are four distinct combinations of signs of the masses, there are four types of nondegenerate critical points designated by M_0 through M_3. Near a local minimum(M_0) or a maximum(M_3), the component of the reduced masses are all positive, and negative, respectively. Near a saddle point(M_1) the reduced masses μ_x and μ_y are positive and μ_z is negative; the saddle point defined by μ_z positive and μ_x and μ_y. negative is designated as M_2. The importance of critical points in all

modulation experiments should now be obvious; a perturbation which changes the density-of-states varies most rapidly with energy, that is, at the critical points themselves. For example, stress and thermal modulation tend to give a derivative-like structure by shifting the energy of a critical point, among other effects. A uniform electric field in effect broadens the zero-field structures, a process which also results in the greatest modifications where the unbroadened function changes most rapidly. So far we have elaborated the theoretical background about why we have sharp and rich traces of structures when we do modulation spectroscopy experiment.

Chapter IV

ER AS A THIRD DERIVATIVE MODULATION SPECTROSCOPY

4.1 INTRODUCTION

So far the general theory of the modulation spectroscopy has been discussed. Now I want to devote myself to low field electroreflectance per se. The electroreflectance technique gives us sharp, well resolved spectra which can be analyzed to get properties of the material. However, ER spectra in general are strongly dependent on the magnitude of the applied field and on experimental conditions, therefore the determination of material parameters from these spectra is a difficult and uncertain process. Still at sufficiently low modulating electric field, ER spectra simplify drastically. These lineshapes have been shown both theoretically and experimentally to be closely related to the third derivative of the unperturbed dielectric function.

This result is particularly significant from a spectroscopic point of view, because third-derivative lineshapes are characterized by the presence of strongly enhanced critical point structures and strongly suppressed background effects. The width of these third derivative critical point structures are determined by lifetime broadening. Consequently, these spectral features are well localized in energy, allowing nearly degenerate critical points to be resolved. Moreover, this localization permits the actual energy band structure in the vicinity of

critical points to be approximated accurately by a simple parabolic density of states, enabling critical point energies and broadening parameters to be obtained directly and precisely from experimental data.

4.2 THEORY

For modulation techniques, the perturbation(the electric field, $\bar{E}$ in electroreflectance) changes the dielectric properties of the unperturbed solid. These changes are described in terms of changes, $\Delta\epsilon(\bar{E})$, of the complex dielectric function, ϵ. In general, both $\Delta\epsilon$ and ϵ are second-rank tensors. The quantity $\Delta\epsilon(\bar{E})$ is obtained by adding a perturbation term, H' to the Hamiltonian, H_0, of the unperturbed crystal and either calculating $\epsilon(\bar{E})$ exactly, in which case $\Delta\epsilon = \epsilon(\bar{E}) - \epsilon(0)$, or calculating $\Delta\epsilon(\bar{E})$ approximately by second-order perturbation theory.

For a uniform electric field, $H' = e\bar{E}.\bar{r}$. It is of fundamental importance that, in contrast to other forms of modulation spectroscopy, the perturbation term $e\bar{E}.\bar{r}$ for the electric field is not lattice-periodic: it represents a net force that accelerates the electron, and it therefore completely destroys the translational invariance of the Hamiltonian in the field direction. This property accounts for the remarkable relationship between low-field ER spectra and the third derivative of the unperturbed dielectric function, which stands in direct contrast to modulation techniques where lattice periodicity is retained and first-derivative spectra are observed.

When the perturbation is an electric field, $H' = e\bar{E}.\bar{r}$ and translation invariance is lost. The electron accelerates and momentum is no longer a good quantum number in the field direction. Consequently, the

one-electron Bloch functions of the unperturbed crystal become mixed. This is equivalent to spreading the formerly sharp vertical transitions over a finite range of initial and final momenta. Besides if the field is not too strong, the mixing will be restricted to those wavefunctions near the originally vertical allowed transition. This will smear out structure in the unperturbed dielectric function, yielding a different and more complicated spectrum having changes in sign. This kind of shape(difference) can be approximated only by higher derivatives of the unperturbed dielectric function. The two zero crossings(typical in ER spectra) are characteristics of the third derivative, as may be verified qualitatively by explicit calculation. Refer Fig.(2).

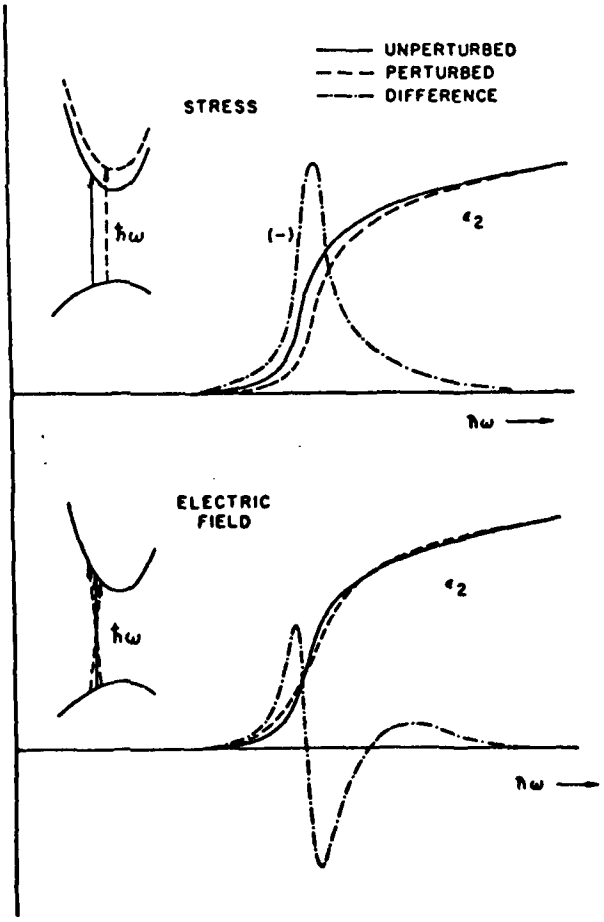

Fig. 2 Top: a schematic diagram of the change in the imaginary part of the dielectric function expected for a first-derivative modulation process where lattice periodicity is preserved. Bottom: similar diagram for electric field modulation where lattice periodicity is not preserved. The effect of the perturbation on the energy band structure and optical transition is shown at the left in each case (after ref. 13).

4.3 THEORETICAL DESCRIPTION

Low field ER spectra are obtained only in that range of externally applied fields where both interband and intraband mechanisms can be treated adequately by first-order perturbation theory. Perturbation theory implies the existence of two energies per mechanism: the characteristic energy of the perturbation and a characteristic energy of the system. The perturbation and system energies for the interband mechanism in ER are eEa_0 (a_0 is a lattice constant), the potential drop across the unit cell, and E_g, the energy separation between the pair of bands under consideration. Clearly, perturbation theory can be applied when $eEa_0 \ll E_g$. The same energy for the intraband mechanism

$$\hbar\Omega = (e^2\bar{E}^2\hbar^2/\mu_\parallel)^{1/3} = [e^2(\bar{E}.\bar{\nabla}_{\bar{k}})^2 E_{cv}(\bar{k})/8]^{1/3} \qquad (51)$$

and Γ, the broadening parameter are less obvious. In Eq.(51), $\mu_\parallel$ is the interband reduced mass of bands c (conduction) and v (valence) evaluated in the field direction, and $E_{cv}(\bar{k})$ is the interband energy at $\bar{k}$. The energy $\hbar\Omega$ is the characteristic energy obtained in the quantum mechanics solution of a particle mass $\mu_\parallel$, which is accelerated in a uniform field of force $e\bar{E}$. Of course perturbation theory will apply to the intraband mechanism when $|\hbar\Omega| \ll \Gamma$. This is more strigent condition than former one. And both conditions are required to apply perturbation theory all the time.

The energies and Γ for the intraband mechanism can be given simple physical meaning by calculating the average energy per particle $\langle\Delta W\rangle$, absorbed in a collision period, τ, for a collection of classical parti-

cles of charge (- e), mass $\mu_{\parallel}$, and zero average initial velocity being accelerated in a uniform field, $\bar{E}$, as discussed qualitatively in the preceding section. Since $dW = \bar{F}.\bar{v}(t)dt$, where $\bar{F} = -e\bar{E}$ and $\bar{v}(t) = \bar{v}_0 + \bar{a}t = \bar{v}_0 - (e\bar{E}/\mu_{\parallel})t$, we have

$$\langle \Delta W \rangle \sim \{\int_0^{\tau} dt\,(-e\bar{E}).[\bar{v}_0 - (e\bar{E}/\mu_{\parallel})\,t]\} = (eE\tau)^2/(2\mu_{\parallel}). \qquad (52)$$

The lifetime, τ, is related to the broadening energy, Γ, by $\tau \sim \hbar/(2\Gamma)$. If we interpret $\langle \Delta W \rangle$ as a field-induced uncertainty in the unperturbed electron energies, by analogy to the interpretation of Γ as a lifetime-induced uncertainties in these levels, then the ratio

$$\langle \Delta W \rangle/\Gamma \sim (eE\hbar)^2/(8\mu_{\parallel}\Gamma^3) = (\hbar\Omega/\Gamma)^3. \qquad (53)$$

Therefore, perturbation theory applies to the intraband mechanism whenever the average energy gained per particle by acceleration in the field is small compared to the natural lifetime-induced uncertainty in the unperturbed electron energy levels.

According to the relative magnitudes of the pairs of characteristic energies there are three ranges of ER as in Table(2) (Aspnes, 1973).

Table 2

Definition and experimentally identifying characteristics of the three ranges of ER spectra in terms of the relative strengths of the perturbation and characteristic system energies for both intraband and interband mechanisms; in the intermediate range, the Airy convolution and Franz-Keldysh approximations assume locally parabolic and completely parabolic energy bands, respectively

Perturbation energy versus system energy			
Range	Intraband (long-range coherent)	Interband (cell-periodic)	Identifying spectral characteristics
High	$\lvert\hbar\Omega\rvert \gtrsim \Gamma$	$e\delta a_0 \sim E_\epsilon$, band structure modified	Stark shifts Selection rules modified
Intermediate (Airy convolution) (Franz-Keldysh)		$e\delta a_0 \ll E_\epsilon$, band structure unchanged	Subsidiary (Franz-Keldysh) oscillations; exponential absorption edge
Low	$\lvert\hbar\Omega\rvert \leq \Gamma/3$		Invariant lineshape scaling as δ^2

For the typical values E=100 kV cm^{-1}, a_0 = 6 Å and $\mu_\parallel = 0.1\ m_e$, we calculate eEa_0 = 6 meV and $\hbar\Omega$ = 21.2 meV (compared to average broadening parameter 80 ~100 meV) for the E_1 transition in MCT.

For a single band pair c, v the intermediate field expression for $\Delta\epsilon$, in terms of general energy band structure defined by $E_{cv}(\bar{k})$, is

$$\Delta\epsilon^{ij}(\bar{E},\Gamma,E) \simeq 4\pi i e^2\hbar^2 p^i_{vc} p^j_{cv}/(mE)^2 (2/(2\pi)^3) \int_{BZ} d^3k \int_0^\infty ds e^{-\Gamma s} e^{iEs} \quad (54a)$$

$$\times \{\exp[-i\int_{-s/2}^{s/2} ds' E_{cv}(\bar{k} - e\bar{E}s')] - \exp[-iE_{cv}(\bar{k})s]\}$$

$$\simeq 4\pi i e^2\hbar^2 p^i_{vc} p^j_{cv}/(mE)^2 (2/(2\pi)^3) \int_{BZ} d^3k \int_0^\infty ds e^{-\Gamma s} \quad (54b)$$

$$\times \exp[i(E - E_{cv}(\bar{k})s]\{\exp[-i(\hbar\Omega(\bar{k}))^3 s^3/3] - 1\}.$$

Eq. (54a) expresses the second-rank tensor, $\Delta\epsilon$, *in component form.* E is the energy of the photon, $\bar{k}$ is the wavevector integrated over the Brillouin zone, s is an integration variable with dimension of inverse energy, $\bar{p}_{cv}$ is the momentum matrix element between valence (v)- and conduction (c)-band states of energy $E_v(\bar{k})$ and $E_c(\bar{k})$ each and Γ is a broadening parameter. The momentum matrix elements are assumed to be independent of $\bar{k}$ in this expression. If the energy bands are further assumed to be locally parabolic, then Eq. (54b) results. This is an integral representation of the Airy convolution expression. If the field is small, the lifetime broadening term exp(-Γs) in Eq. (51b) will cut off the integrand before the term $\exp[-i(\hbar\Omega s)^3] \simeq 1 - i(\hbar\Omega s)^3/3 + \ldots$ changes appreciably, since $(\hbar\Omega)^3 \sim E^3$. The leading term in this expansion simply yields, and cancels, the unperturbed dielectric function.

If $|\hbar\Omega| < \Gamma/3$, it has been shown that the higher-order terms may be neglected (Aspnes, 1970, 1972b). After explicit integration we find the low-field expressions

$$\Delta\epsilon^{ij}(\bar{E},\Gamma,E) \simeq (8\pi e^2\hbar^2 p^i_{vc} p^j_{cv}/(mE)^2)(2/(2\pi)^3) \tag{55a}$$

$$\times \int_{BZ} d^3k\,(\hbar\Omega)^3/(E_{cv}(\bar{k}) - E - i\Gamma)^4$$

$$\simeq ((\hbar\Omega)^3/3E^2)(\partial^3/\partial E^3)(E^2\epsilon^{ij}(\Gamma,E)) \tag{55b}$$

$$= (e^2\hbar^2\bar{E}^k\bar{E}^l/24E^2)(\mu^{-1})^{kl}(\partial^3/\partial E^3)(E^2\epsilon^{ij}(\Gamma,E)). \tag{55c}$$

[summation over repeated indices is assumed in Eq. (55c) and throughout.] Eqs. (55b) and (55c) show clearly the third-derivative relationship between the field-induced change, $\Delta\epsilon$, and the unperturbed dielectric function, ϵ. This follows mathematically because multiplication of the integrand in Eq. (54a) by s^n is operationally equivalent to calculating $E^{-2}(\partial^n/\partial E^n)\,[E^2\Delta\epsilon^{ij}]$.

4.4 SCHOTTKY BARRIER

When a semiconductor is brought into contact with a metal we have a barrier layer in the semiconductor where charge carriers are severely depleted. This barrier is also called a depletion layer or exhaustion layer. In Fig. (3) an n-type semiconductor is brought into contact with a metal. Fermi levels are equalized after the transfer of electrons from the conduction band of the semiconductor to the metal due to chemical potential difference. Positively charged donor ions are

left behind in this region that is practically stripped of electrons. Its width greatly exceeds the electron mean free path. Therefore resistance is very high in this region.

Here the Poisson equation is

$$\text{div } \bar{D} = 4\pi Ne, \tag{56}$$

where N is the donor concentration. The electrostatic potential is determined by

$$d\phi^2/dx^2 = - 4\pi Ne/\epsilon \tag{57}$$

which has a solution of the form

$$\phi = - 2\pi Nex^2/\epsilon. \tag{58}$$

To make the theory simple we deal with the equation dimensionally. When ϕ is divided by x we get E(electric field). Multiplying both sides by V_m(applied modulation voltage) and dividing by x we get

$$E^2 \propto - 2\pi NeV_m/\epsilon. \tag{59}$$

According to Eq.(55) we can see that $\Delta\epsilon \propto E^2 \propto V_m$. Invoking Eq.(42), Eq.(55) and Eq.(59) we get

$$\Delta R/R \propto - ANeV_mL. \tag{60}$$

where L is the line shape function characteristic of a material and A is a constant. We can see that $\Delta R/R$ is proportional to the number of carriers as well as applied modulation voltage.

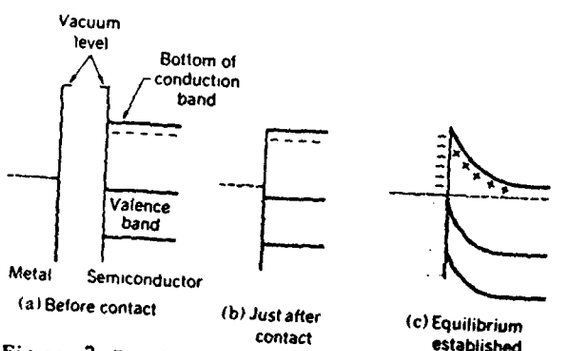

Figure 3 Rectifying barrier between a metal and a n-type semiconductor. The Fermi level is shown as a broken line.

Chapter V

CONNECTION BETWEEN $\Delta R/R$ AND $\Delta\epsilon$

5.1 BRIEF INTRODUCTION

The quantity $\Delta\epsilon$ given in Eqs. (54) and (55) can be related to the experimentally measured relative change in reflectivity (Aspnes, 1973), $\Delta R/R$, by

$$\Delta R/R = \mathrm{Re}[C_s C_{ex} C_{in} e^i e^j \Delta\epsilon^{ij}], \tag{61}$$

where

$$C_s = 2n_a/[n(\epsilon - \epsilon_a)], \tag{62}$$

$$C_{ex} = [1 - g(\epsilon - 1)]^2, \qquad g \leq 0, \tag{63}$$

$$C_{in} = -2ik\int_{-\infty}^{0} dz' e^{-2ikz'} [\bar{E}(z')/\bar{E}(0)]^2, \tag{64}$$

and e^i, e^j represent Cartesian components of the unit polarization vector, $\hat{e}$. The factor $C_s = \alpha - i\beta$ gives the Seraphin cofficient, α and β, for a two-phase interface (ambient $n_a^2 = \epsilon_a$, unperturbed substance $n^2 = \epsilon$), rewritten in complex variable form for convenience. C_{ex} represent the electron-hole Coulomb interaction in the contact exciton approximation, and C_{in} is the factor arising from spatial depen-

dence, or inhomogeneities, in the perturbing field. In Eq.(63), ϵ is the measured dielectric function, which is assumed for simplicity to be a scalar. In Eq.(63), g is the strength parameter, which can be assumed to be constant for a given structure. Eq.(64) has been written explicitly for the low-field limit. In Eq.(64), $k = n\omega/c$ is the propagation parameter of the light in the substrate.

5.2 SIMPLE PARABOLIC MODEL DENSITY OF STATES

The strong localization of low field ER structure of a single critical point to within an energy range not exceeding several broadening parameters is important for spectroscopic purposes, for it means that actual energy band structure in vicinity of a critical point can usually be replaced accurately with a simple parabolic model, thereby simplifying the analysis of experimental spectra for band structure. For one-, two-, and three-dimensional simple parabolic model densities of state (D = 1, 2, and 3, respectively), Eq.(54a) become

$$D=1: \quad \Delta\epsilon^{ij} = (5i^{1-}/8)\,(|2\mu_x/\hbar^2|^{1/2}K_yK_z)\,Q^{ij}\bar{E}^2\,(E - E_g + i\Gamma)^{-7/2} \tag{65a}$$

$$D=2: \quad \Delta\epsilon^{ij} = (2i^{1-2/3})\,(|4\mu_x\mu_y/\hbar^4|^{1/2}K_z)\,Q^{ij}\bar{E}^2\,(E - E_g + i\Gamma)^{3}, \tag{65b}$$

$$D=3: \quad \Delta\epsilon^{ij} = (\pi i^{1-3/4})\,(|8\mu_x\mu_y\mu_z/\hbar^6|^{1/2})\,Q^{ij}\bar{E}^2\,(E - E_g + i\Gamma)^{5/2} \tag{65c}$$

where

$$Q^{ij} = e^4\hbar^4P^i_{vc}P^j_{cv}/8\pi\mu_{\parallel}E^2m^2.$$

l is the order of the critical point, equal to the number of negative effective masses μ_x, μ_y, μ_z; k_y and k_z represent k space cutoff limits used for D = 1 or D = 2; $\mu_\parallel$ is the interband reduced mass evaluated in the field direction as defined in Eq.(51). In this simple model Γ, E_g, and phase factor can be determined from an experimentally determined spectrum $\Delta\epsilon$ without requiring the value of $\bar{E}$.

If the dielectric function ϵ is a slowly varying function of energy in the vicinity of the critical point structure, Eqs.(62), (63), (64) show that the three major interactions that take $\Delta\epsilon$ into the experimentally measured lineshape $\Delta R/R$ (the optical properties of the ambient and material, electron-hole interaction, and field inhomogeneities) affect only the amplitude and phase factors, and again leave the energy location and width of the structure unchanged(This is the important point for characterization of MCT). This means that critical point energies and broadening parameters can also be obtained directly from experimental lineshapes $\Delta R/R$, without requiring data reduction by means of Kramers-Kronig analysis, of a knowledge of the field homogeneity, electron-hole interaction strength, or the optical properties of the material.

5.3 DETERMINATION OF BAND STRUCTURE PARAMETERS BY FITTING

ER spectra in general, and low-field spectra in particular, exhibit one positive and one negative extremum for each critical point. This is a general property of complex resonance lineshapes of the form

$$\Delta R/R = \mathrm{Re}[Ce^{i\theta}(E - E_g + i\Gamma)^{-n}] \qquad (66)$$

where C and θ are amplitude and phase factors that vary slowly with E, and $n \geq 2$. Here the amplitude and phase factors C and θ determine the amplitude and asymmetry of the lineshape, respectively, and E_g and Γ determine the energy location and width of the structure. Clearly, the amplitude factor only scales the lineshape determined by θ, n, E_g, and Γ and thus does not enter into the actual lineshape determination. Note, however, that regardless of the value θ the energy gap always lies between the two extrema and the energy separation between the two extrema is nearly constant.

This observation suggests that E_g and Γ should be obtainable relatively simply from these lineshapes. The key to determining E_g and Γ directly from experimental lineshapes lies in the fact that the ratio of the absolute magnitudes of the positive and negative extrema (the asymmetry of the lineshape with respect to the baseline) uniquely determines the phase factor, θ. Once θ is known, the systematics of the lineshape allow Γ to be related precisely to the energy separation between the positive and negative extrema and also allow the energy gap, E_g, to be located precisely between the two extrema. Note also the dominant lineshape-determining processes, the critical point type, optical constant, field inhomogeneity, and electron-hole interaction in the contact exciton approximation, contribute only to the amplitude and phase factors C and θ. Since θ can be determined from the asymmetry of an experimental lineshape, it follows that a detailed knowledge of each interaction is not necessary to determine E_g and Γ and that these parameters can be determined directly from the experimental lineshapes themselves by fitting. Fig.(4).

SAMPLE FITTING

```
MCT63 ZO=1V V=2V S=1MV P=0 KOH 140 SEC .2% BR SYS B 3/16/84
    SIGMA          C          DE1          DGAM      DSIGMA2        OFFSET
     0.06       9.110       31.115         0.000       0.534          0.00
     0.22      28.109       -3.101         0.000       0.610          0.00
    THETA          EG        GAMMA
    6.145       2.417         0.099
    6.896       3.866         0.171
THE VALUE OF R IS              0          THE INTERSECT ENERGY IS     2.59
THE VALUE OF X IS              0.343
THE ETCH DEPTH IS     9.800 MICRONS
```

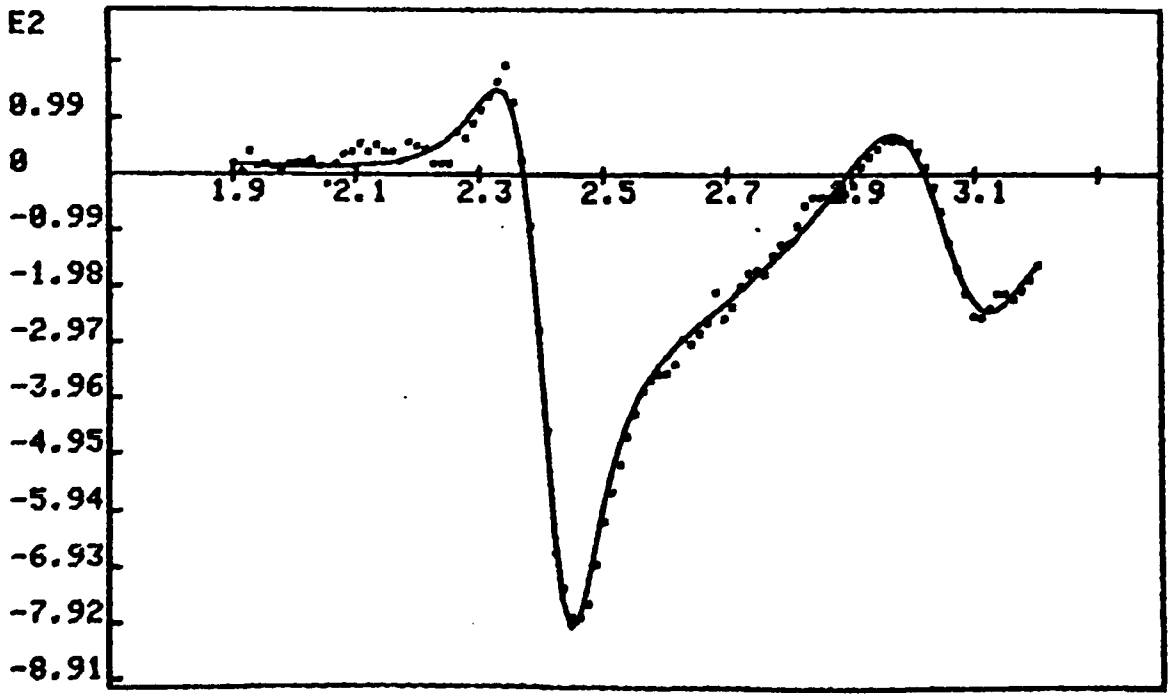

Fig. 4 ..... experimental

——— theoretical

Chapter VI

EXPERIMENTAL SETUP FOR EER

6.1 INTRODUCTION

The block diagram of EER setup is shown in Fig.(5). For the light source, we have used a 150W Xe compact arc-lamp which gives us a wide range of wavelengths. That light is incident on the grating monochromator (GCA/McPHERSON, model EU-700-56) which is computer controlled to achieve the desired wavelength intervals during the run.

The sample is mounted on the sample holder (nylon) with polystylene Q-dope. The sample holder, which is shown Fig.(6), consists of two sections sealed together with wax in such a manner as to form a hollow interior. Electrical contact on the sample is achieved through the use of two platinum electrodes which are placed in electrolyte solutions which, while electrically insulated, are in contact with the front and rear surfaces of the sample respectively. One electrode is dipped into REG electrolyte (made of 1 gram of Tetraethylammonium Perchlorate ($(C_2H_5)_4NClO_4$) into 200 ml of propylene carbonate ($OCH(CH_3)CH_2OCO$)) in the inside of the sample holder. The other electrode is immersed in electrolyte in a quartz cell which is external to the sample holder. Depending on the purpose we use various kinds of electrolytes, such as KOH (.1 N), Lactic acid (10 %, $C_3H_6O_3$), etc.

A modulating electric field (at some frequency, f) is applied to the sample by an HP 3310A function generator which also puts out dc voltages as well. Since exit flux of intensity I_o is focused on the sample, the reflected intensity will therefore contain a dc or average value, I_oR, and a modulated value, $I_o\Delta R$, that varies in phase with supplied electric field (frequency, f) by function generator.

In our system an anode current regulator for the photomultiplier tube has been employed to maintain constant R, ΔR, therefore, is the only quantity that varies, and measurements of it can be made with a lock-in amplifier. The exit beam is focused on the sample using a f=100 mm UV lens. Light reflected from the sample is collected with other f=100 mm UV lens and measured with a photomultiplier tube.

EXPERIMENTAL SETUP FOR EER

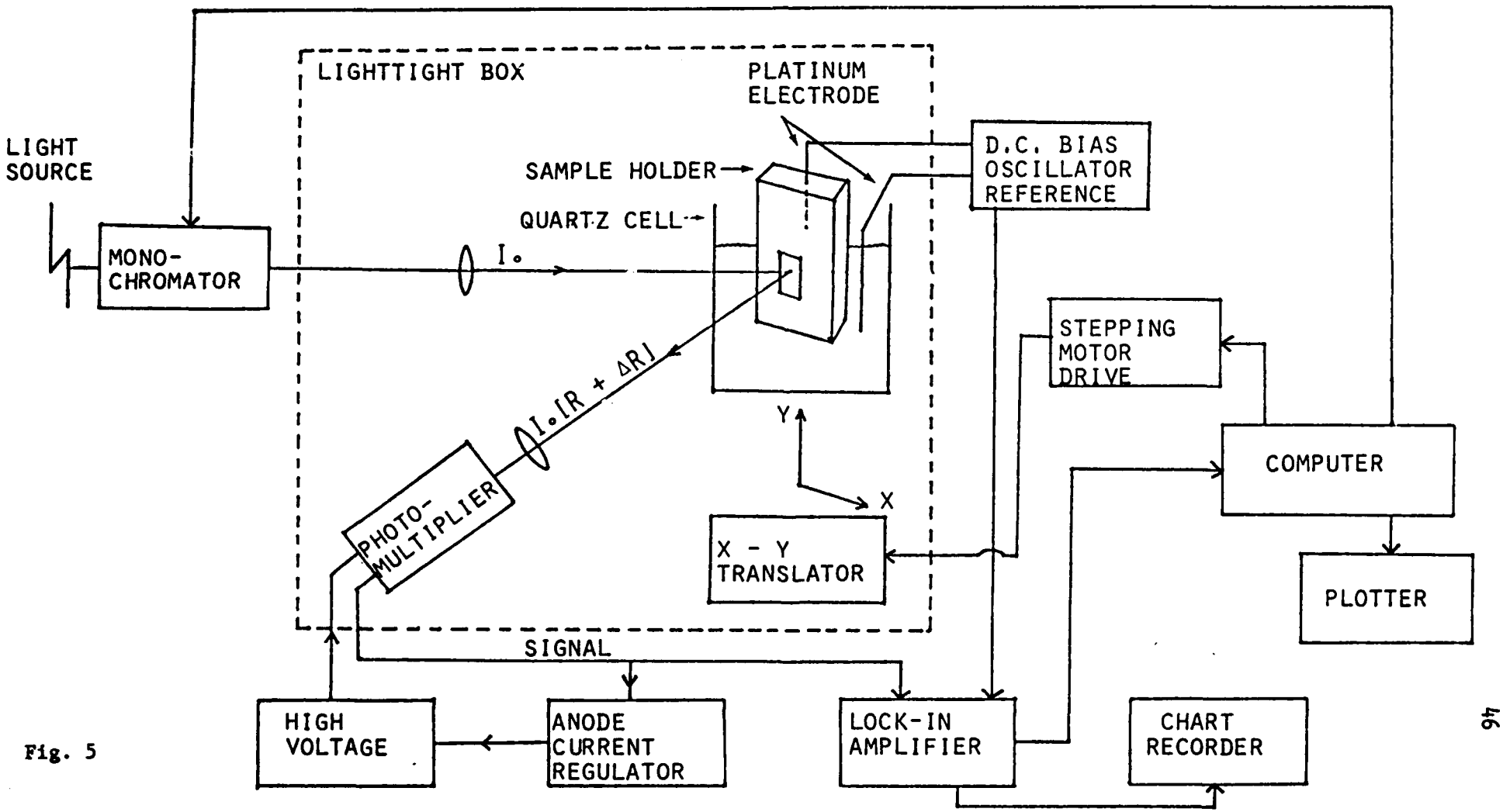

Fig. 5

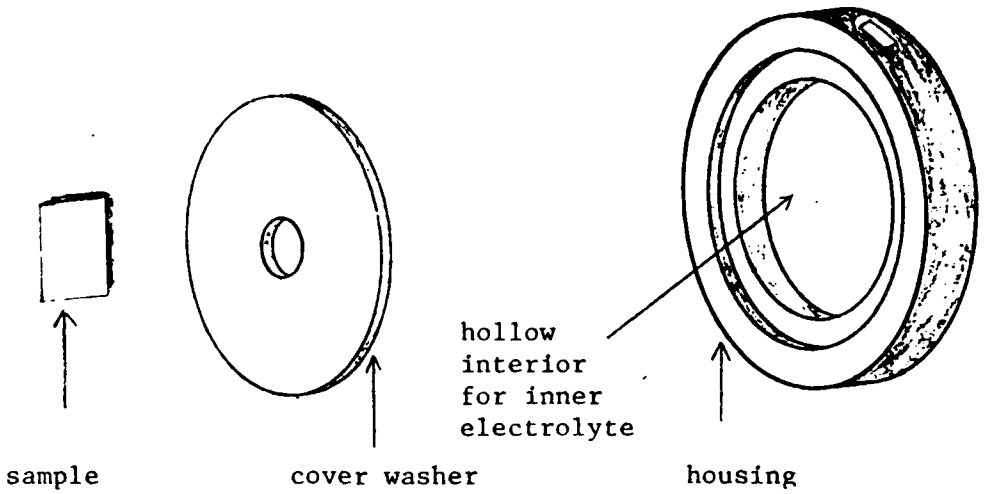

FOR FRONT SURFACE

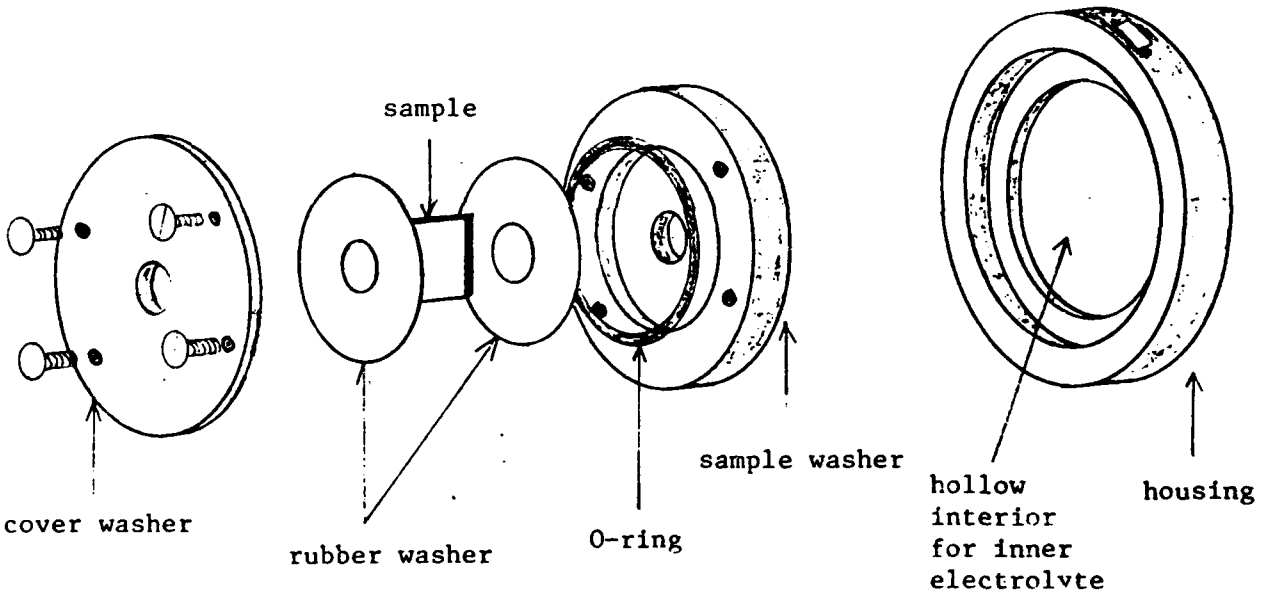

FOR BOTH SURFACES

Fig. 6 Sample Holder

SAMPLE LINESHAPE BY EER

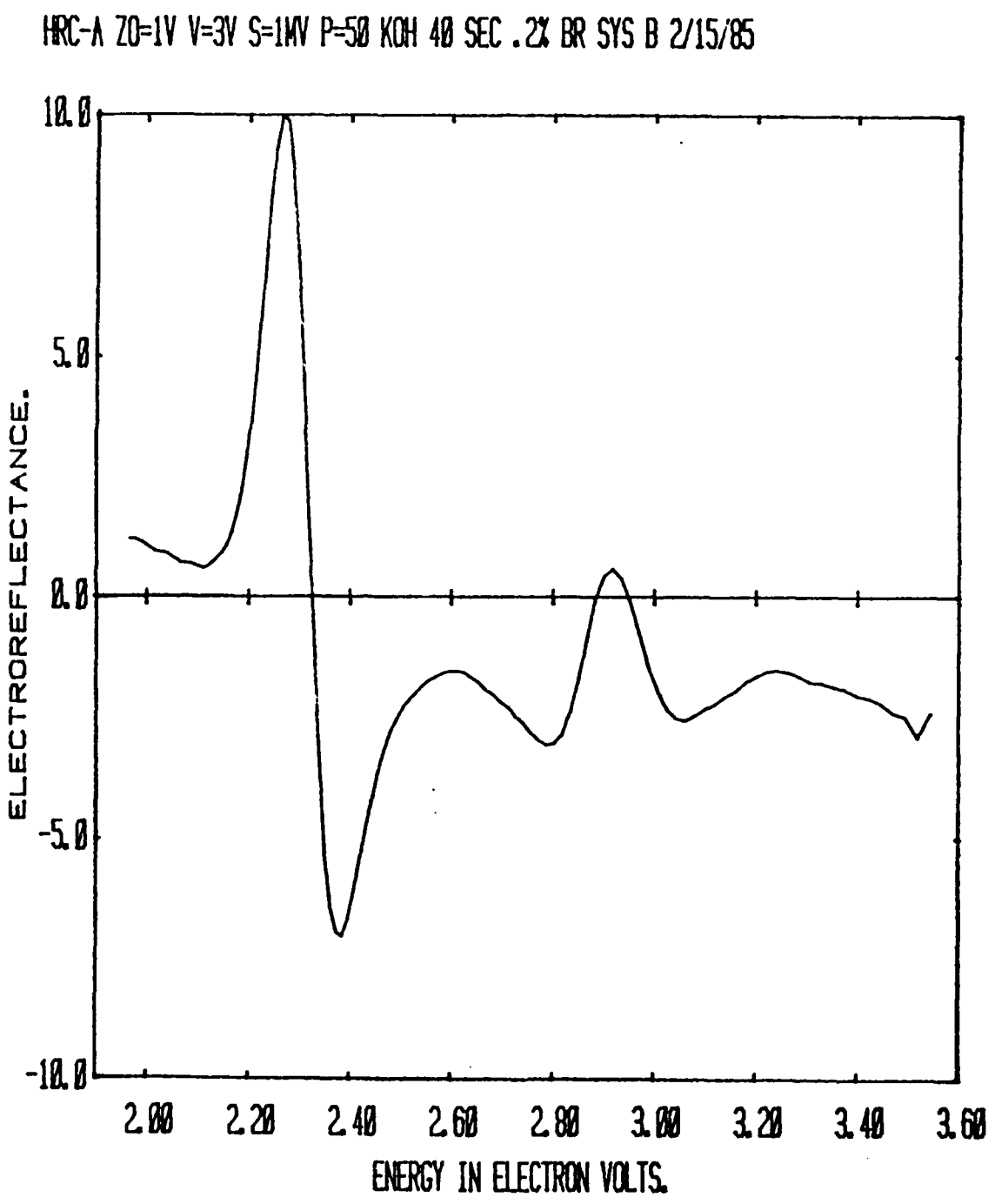

Fig. 7

6.2 SAMPLE PREPARATION AND RUN

i) mono scan

After preparing proper size samples by cutting (and polishings when the surface is dirty or doesn't give a signal initially) the sample is mounted and introduced to the electrolyte environment as depicted in Fig.5. Proper electrical contact is ensured by measuring resistance between two platinum electrodes. This is a crucial test since leaking between sample and cover washer (Fig.6) will defeat the modulating electric field on the sample. Measured resistances less than .3 MΩ suggest possible leakage and call for a visible inspection of the seal. Experience also shows that for MCT the normal resistance range to obtain a signal is .5 MΩ to 7 MΩ. If the measured resistance is greater than 10 MΩ, the chance to get a signal is very small and for higher resistances in the range of 20 MΩ it is almost impossible.

Our EER setup is fully computerized as far as the experimental run is concerned. By selecting the scanning range, wavelength interval, desired readings, and distance between points (area scan only), the computer will control the monochromator, record the data from lock-in amplifier, and plot the lineshape on the plotter.

ii) area scan

Area scan is an application of the mono scan used to investigate the uniformity of sample throughout the surface. In this case the computer has one more duty to perform - laterally translating the sample. In this manner various sample positions can be probed and lineshapes ob-

tained for each position. Before we try the area scan we need a mono scan data. The wavelength scanning range, which must include either a peak point or a zero crossing point, is first established by recording a mono scan. In the area scan, the computer will record either one peak point or one zero crossing point for each spot of the sample. Since each point is proportional to E_1, we can determine the uniformity of the surface by the area scan. Scanning time, however, is long.

6.3 DATA PROCESSING

When enough data are taken we use the computer to fit the data to get energy gap, linewidth, phase angle(mono scan only). The number of data taken depends on the purpose of the experiment. We have developed the full lineshape fitting to get better E_1 value as well as better Γ value. The energy fitting range of MCT was usually from 1.8 eV to 2.5 eV which includes the E_1 energy transition for MCT. Theoretical discussion is done in Chapter 5 and more will be done in Chapter 9. Specially in Chapter 9 we have the generalized theory which fits the lineshape for whole energy range.

6.4 ACCOMPLISHMENTS

By exploiting the EER technique I have made several important contributions to the characterization of MCT.

1. A more reliable relationship between E_1 and the alloy composition of Cd in MCT has been established by carefully determining the coefficients in the expression $E_1 = a + bx + cx^2$.

Even though the quadratic relationship between the alloy composition x and the interband transition energy E_1 is well known, the parameters measured do not agree one another. Therefore the establishment of sound values for parameters has been an important contribution of mine for the characterization of MCT. For this I have used defect-free MCT(x=.5), HgTe(x=0), and CdTe(x=1) and measured exact E_1 values by using full lineshape fitting to determine accurate parameters. I find that a=2.135, b=.600, c=.640.

II. The etching rate for MCT by Br/Me has been carefully calibrated.

For a reliable profiling of MCT we need to know the exact etching rate of an agent, in our case Br/Me, so that we can tell how much we take off when the sample is etched. But the etching rate of the Br/Me depends on concentration of agent and etching time. In addition to these factors the mixture of Br/Me is not stable at all. To reduce the effect of the instability of the agent we made the mixture just before the actual etching. By taking into account all these factors I found the calibrated etching rate to be 1400 Å per 1 minute jetting with .2% Br/Me agent.

III. The profiling technique, which employs the calibrated etching rate and the established relationship between E_1 and x, has been developed.

Since I have established accurately the E_1 and x relationship and the etching rate for MCT, the profiling of MCT is a natural application of the two accomplishments. By fitting EER lineshapes to determine E_1

at each predetermined crystal depth that is achieved via etching the E_1 versus x relationship was used to establish the composition of Cd as a function of crystal depth.

IV. MCT type conversion due to stress has been discovered.

Because of the fragility of the MCT it is very important to know the effect of mechanical shock on the MCT. By collaborating with Stanford(W. E. Spicer et al 1983) the type conversion of MCT due to stress has been confirmed.

This summarizes the work that I have carried out independently. The extensive amount of data recorded, however, has led to additional findings. For severely defectuous samples the theoretical lineshape was incapable of fitting the data except for energies very near the critical point energy E_1. This prompted the initiation of a theoretical investigation into the importance of new defect-enhanced physical effects in EER not described in the theory of Aspnes(1973). The generalized theory of Raccah et al.(1985) resulted. Our data has been instrumental in confirming the validity of this generalized theory.

Chapter VII

CHARACTERIZATION OF MCT BY EER

7.1 THEORY

Electrolyte electroreflectance(EER), being a derivative technique, is a preferable method to simple reflectance because of its greater sensitivity and simplicity. It yields spectra which can be fitted to a theoretical expression and the fit determines, in addition to the interband transition energy E_1, two very useful parameters, namely, EER linewidth Γ and phase angle θ.

It is well known that in alloys, E_1 is related to the composition x of alloy by a quadratic expression of the type:

$$E_1 = a + bx + cx^2. \tag{67}$$

The parameters are determined empirical and c is called the bowing parameter. It has been determined numerous times for $Hg_{1-x}Cd_xTe$ (MCT) but the published values are in very poor agreement with one another(Kisiel, 1971; Moritani, 1973; Casula, 1977; Podgorny, 1979). The usefulness of EER, when applied to alloys, depends largely on the reliability of the $E_1 = F(x)$ relationship. Therefore, The main efforts have been directed towards establishing more accurate values of the parameters. For this purpose E_1 values of the end members, CdTe and HgTe, have been obtained. Also E_1 values on high quality samples of the al-

loys with accurately determined composition close to x = 0.5, where the bowing is maximum, have been calculated by fitting. In all cases the interband transition energy E_1 has been determined both by EER through lineshape analysis, and by Automatic Scanning Ellipsometry (ASE). In the latter case one fits the third derivative of the spectrum of the imaginary part of the dielectric function. The values of E_1, which have been determined for x = 1, 0.5, and 0 were 3.375, 2.595, 2.135 eV, respectively, in good agreement with other recent work. These results in turn yielded c = 0.640 with an uncertainty of C.05. The other parameters are a = 2.135, and b = .600.

Comparison to previous results is difficult because the value of c depends greatly on that of E_1 for the end members and, in this respect, the accuracy of the previous work was less than ours. They did not in general use a modulation spectroscopic method and when they did they did not carry out a full lineshape analysis which is much more accurate. It is worth mentioning, however, that the value determined is not in agreement with the prediction of Van Vechten's dielectric theory(1970), which is c = .38, but then neither was that of Moritani(1973), which was c = 0.84.

It is believed that this new expression is more reliable than any previously published. These numbers have been checked against numerous samples of varied origins, including materials of reasonable quality, where the value of E_1 can be determined to an accuracy of 0.003 eV by fitting of the EER lineshape which yields x with an uncertainty of 0.004 only. The linewidth Γ is obviously affected by all scattering processes and its relationship to the etch pit density revealed by micrographic

examination, i.e., its relationship to scattering by structural defects, has been investigated. The magnitude of the linewidth is an indication of the defect density of the materials.

7.2 ETCHING

The etching rate of the MCT with etching agent, Br/Met, has been established. The etching rate is about 1400 Å by 1 min. jetting with .2% Br/MET agent. By adjusting jetting time and concentration of agent we can etch a certain amount of depth everytime. EER lineshape data can be taken each time after successive etchings. By fitting the lineshape x values at various depths of the sample one can obtain a relation between x and depth. This graph of x vs depth shows us the quality of material depthwise(Fig.8). Similar x determinations at various surface locations can be obtained by laterally moving the sample with a translator. In this manner information about the lateral uniformity is provided(Fig.9).

Sample x vs depth graph (MCT)

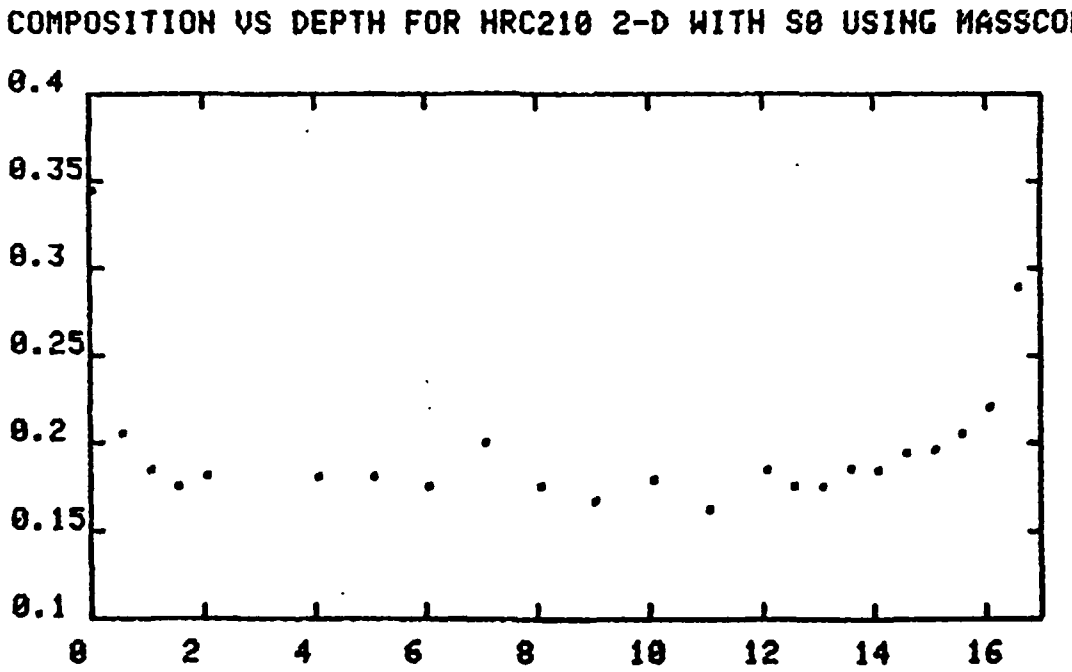

Fig. 8

02 20=1V V=1V S=.1MV P=120 REG ZERO XING VS X,Y SYS A 9/8/81
MAXIMUM SCALE FACTOR = 0.04

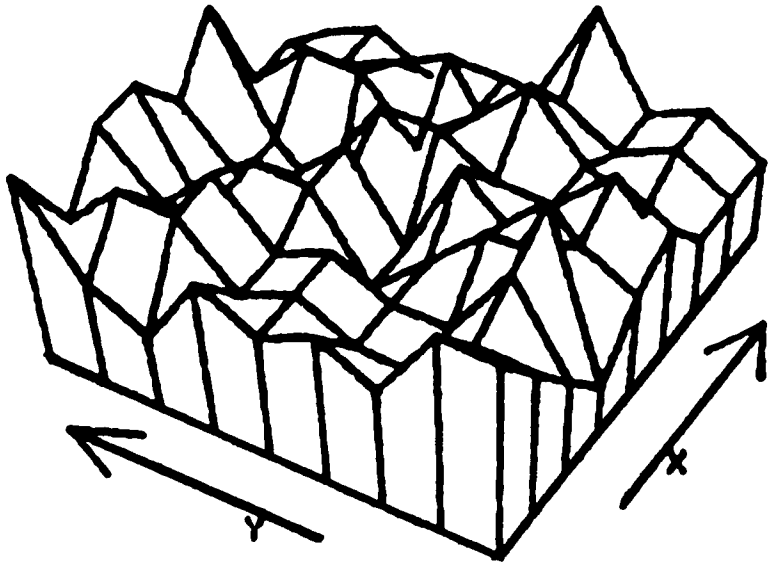

Fig. 9 Area Scan

7.3 RESULT OF BULK MCT

In chapter 9 it will be described how p-type MCT can be converted to n-type by stress and that the stressed volume is depleted in mercury. Ion implantation of p-type MCT surfaces converts them to n-type, with the p/n junction buried 1.5 microns below the surface. Impurity profiling, however, shows that the implant penetration is no greater than .15 micron. The type conversion must, therefore, result from the damage induced by the implantation rather than from the activation of the implant.

On the other hand, the mercury depletion of the stressed volume is in agreement with the energy dispersive x-ray analysis, in transmission electron microscopy, which shows selective motions of mercury in localized defects zones (Magee, T. J., 1982)

It seems to us that these results shed new light and help in understanding the effect on the crystals of the mercury vapor anneal, particularly on n-type MCT. According to conventional understanding, the anneal fills in mercury vacancies and confers to the annealed material a greater structural perfection. The n-type character is then due to the ppms of excess mercury atoms which are acting as donors. In view of the fact that structural defects are perfectly capable of conferring an n-type character to MCT and that mercury tends to diffuse along defects lines, it is clear that a wholly opposite interpretation could be given. Namely that the mercury vapor anneal, far from yielding a more perfect crystal, generates instead, new defects which in turn render the material n-type.

In general EER results, whether obtained on bulk single crystals or on epilayers, are consistent with this picture. When comparisons of surfaces prepared in the same way, whether by us or by someone else, and including those which by present standards of the surface treatment are considered optimal, the p-type materials always exhibit a narrower linewidth Γ than the n-type materials. Therefore, it is believed that p-type materials have intrinsically less in structural defects.

Independent from these observations, we have already found that Bromine/methanol (Br/Met) attack leaves MCT surfaces depleted in cadmium and more defective. In view of what has been said above these statements bear reexamining. The EER signal is due to the modulation of the optical absorption of material by the applied electric field. In this picture, neutral structural defects will act primarily as scattering centers and will be perceived through their effects on the broadening parameter Γ. For obvious reasons the third derivative of the optical spectra obtained by automatic scanning ellisometry (ASE) will be similarly affected. On the other hand charged defects will not interact with the polarization of light (ASE) anymore than would neutral defects while they will interact very strongly with an applied electric field (EER) to which, in first approximation, neutral defects would be unaffected. It is therefore predictable that charged defects will play an insignificant role in ASE spectra while their role could be greatly emphasized in EER spectra.

This is easily understood when it is recalled that in EER experiment the modulating electric field is applied via a Schottky barrier and charged defects would affect that Schottky barrier just as much as they

would affect any other device one would attempt to build on that surface. For this reason it has always been difficult to study by EER materials which are prone to exhibit a high density of surface states or of charged defects without some means to "heal" or relax the surface. For just about all semiconductors the problem does not present itself but for freshly etched MCT it is definitely there.

It is this effect that has been found earlier in qualitative terms and which has taught us never to study by EER an etched MCT surface before it has been "healed" by electroetching or by anodization. This analysis has recently received support from comparative measurement made in our laboratory and elsewhere. It would indeed appear as if Br/Met attack does not affect the ASE spectra while it does affect the EER spectra obtained before electroetch or anodization. Moreover the effect of the Br/Met attack seems to be considerably greater on n-type samples than on p-type samples, consistent with our hypothesis of the greater density of charged defects in n-type materials. The above results as well as their interpretation are very tentative and are presented here primarily because of the difference between the n-type and p-type responses.

7.4 LIQUID PHASE EPITAXY (LPE)

Liquid Phase Epitaxy (LPE) is a logical approach to a better control of the growth process. The growth takes places primarily at the bath/crystal interface and ideally can be efficiently regulated. From an analytical point of view, the depth profile of an epilayer is a frozen-in record of interfacial history and its study is of obvious significance to the understanding of growth mechanism.

Several techniques are used to acquire this information and they are EER, the SIMS (Secondary Ion Mass Spectrometer) and the microprobe. More than one hundred samples of all origins have been studied mostly by EER. The key condition to the application of EER to the profiling of LPE materials is a calibrated etch rate since accurate knowledge of the depth of material removed before each EER spectra taken is essential. Using conventional techniques, it is possible to etch down the entire surface of our samples (usually 3 x 4 mm) with a depth control of approximately 200 Å and with reasonable uniformity. This precision matches well the light penetration, which is only 300 Å, and makes of EER a tool uniquely suited to the characterization of LPE materials.

The calibration was established by etching layers of known thickness in steps of 0.5 micron and determining the value of E_1 at each depth by a fit of EER spectrum. When it reached the value of 3.375 eV, which is determined to be characteristic value of CdTe the substrate had become exposed. In all cases the thickness of the film had been very accurately determined beforehand by analysis of the infrared (IR) interferences obtained by transmission through the layer. It has allowed us to determine the depth profiles previously described as well as the composition and defects density, of numerous epilayers. Samples from essentially all of the active growth laboratories were included and a summary of principal results of the investigation is presented here.

In general the profile in composition of a layer exhibits four distinct regions which are:

1) The Near Surface Region (NSR),

2) The Bulk Region (BR),

3) The InterDiffusion Region (IDR),

4) The InterFacial Region (IFR),

The first of them, i.e., the NSR, is generally graded and low in cadmium; it is always removed before making use of the layer. Its depth depends very much on the growth technique but averages around two microns and it has been found that the NSR is very rich in defects as was already shown.

The BR is of course better behaved and, in good epilayers, is uniform in composition to within 0.01 in x. For comparison, this control of x would need to be lowered to 0.004 if it were to match the quality of state of the art bulk materials. The depth of this region depends on the thickness of the layer but will typically be of the order of 12 microns in a 20 microns layer. The defects density is usually the lowest in the BR and averages 5×10^5 etch pits/cm^2 in recent samples.

The IDR and the IFR, which were prominent features in early LPE samples when preparation of the substrates was not as skilled as it now is have all but disappeared in state of the art LPE materials. When seen they have typical depths of four and two microns, respectively, in epilayers of 20 microns. The cadmium content increases, as expected, in both these regions, slowly in the IDR and very rapidly in the IFR. As an example in a layer, where the nominal composition is $x = 0.20$, it would rise to $x = .25$ within the IDR and from there to $x = 1$ within the IFR. Obviously these regions are more defective than the BR, however they can be greatly improved by a suitable preparation of the substrates, as has already been shown.

The results shown in Fig.(10) are meant to illustrate the significance of proper substrate preparation. They compare two layers grown in the same laboratory and by identical procedures, the only difference is that in one case the surface preparation of the substrate was conventional, while in the other it was achieved by hydroplaning. And it clearly shows that hydroplaning method is much better than conventional technique.

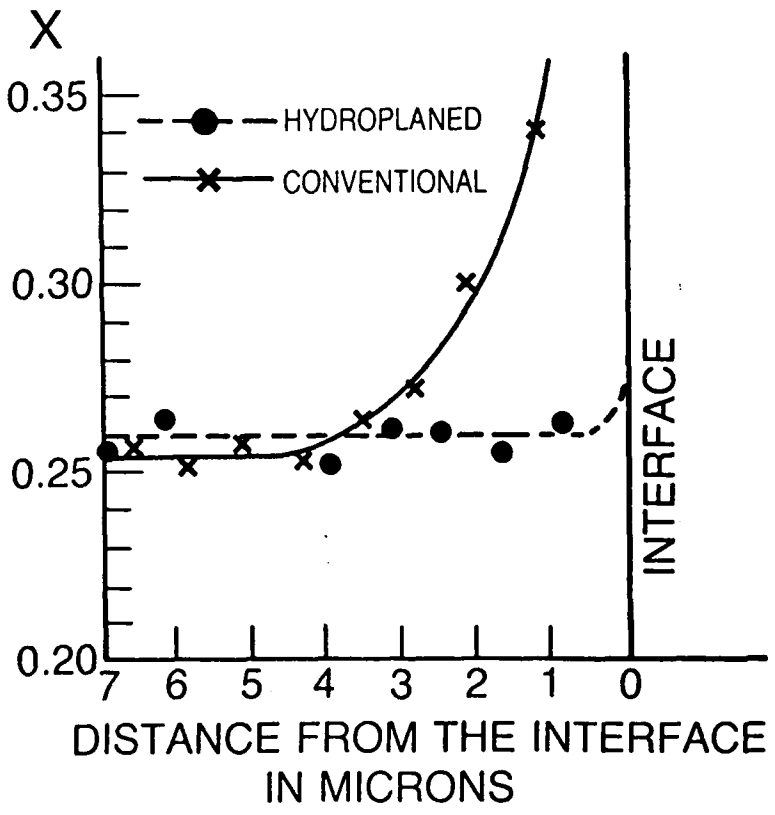

Fig. 10 Comparison of two epilayer/substrate interface. Substrates are prepared by different methods.

The SIMS is a popular technique to detect the presence of impurity traces and to determine their profiles. The SIMS profile of representative MCT sample, which had already been profiled by EER, is shown in Fig.(11) together with the EER profile. One can see that qualitatively there is reasonable agreement between the two techniques. In Fig.(12) I showed the position of E_1 transition in Brillouin zone for MCT. I have chosen the E_1 transition energy range to work with for MCT EER because it lies in the visible light range, varies substantially with the Cd concentration x, and gives rise to strong structure in both EER and ASE. Most of all this critical point is in the (111) direction which coincides with chemical bonding direction. Therefore this range is very sensitive to defects.

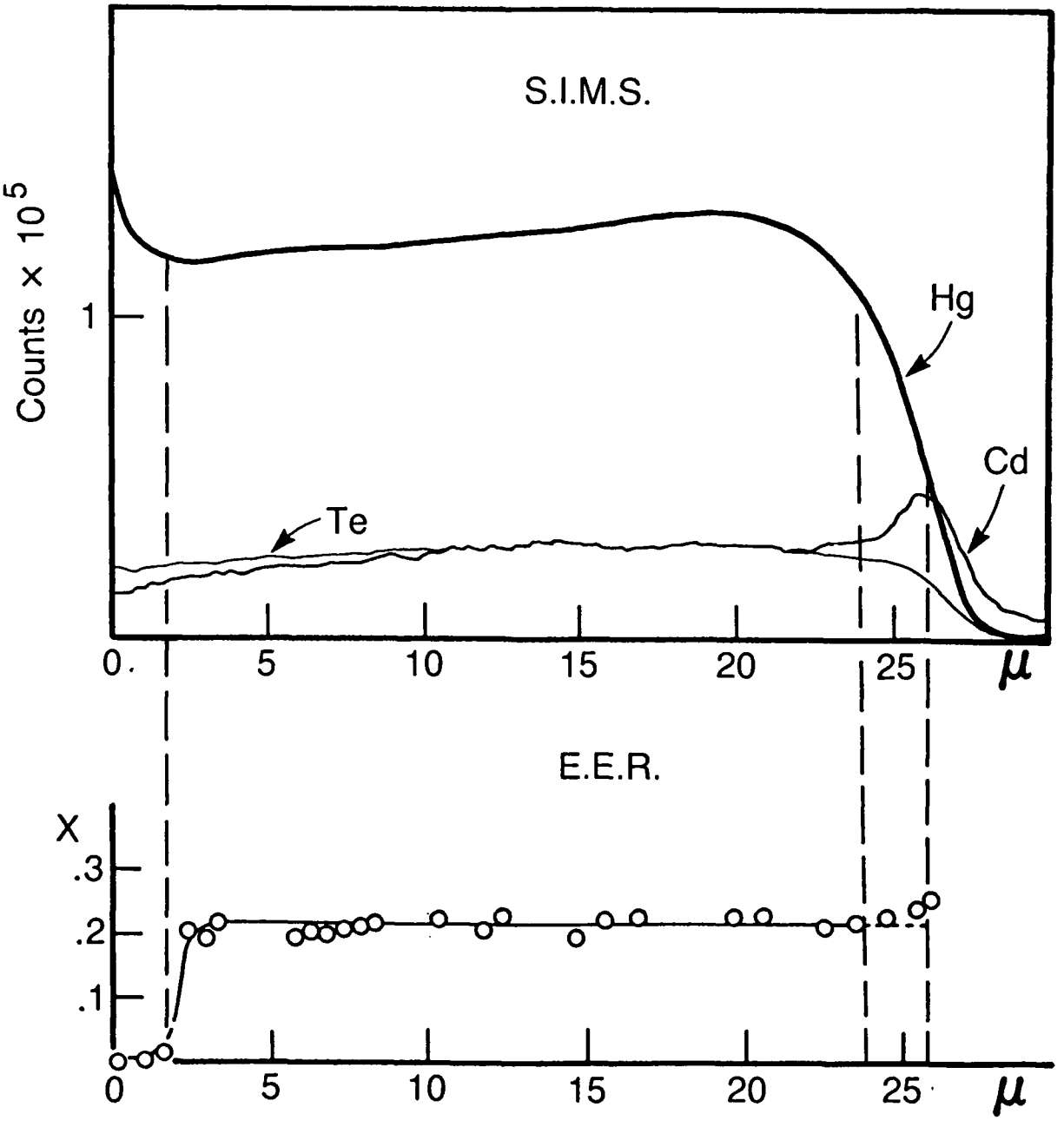

Fig. 11 Comparison of SIMS and EER profiles

SCHEMATIC BAND STRUCTURES OF $Hg_{1-x}Cd_xTe$

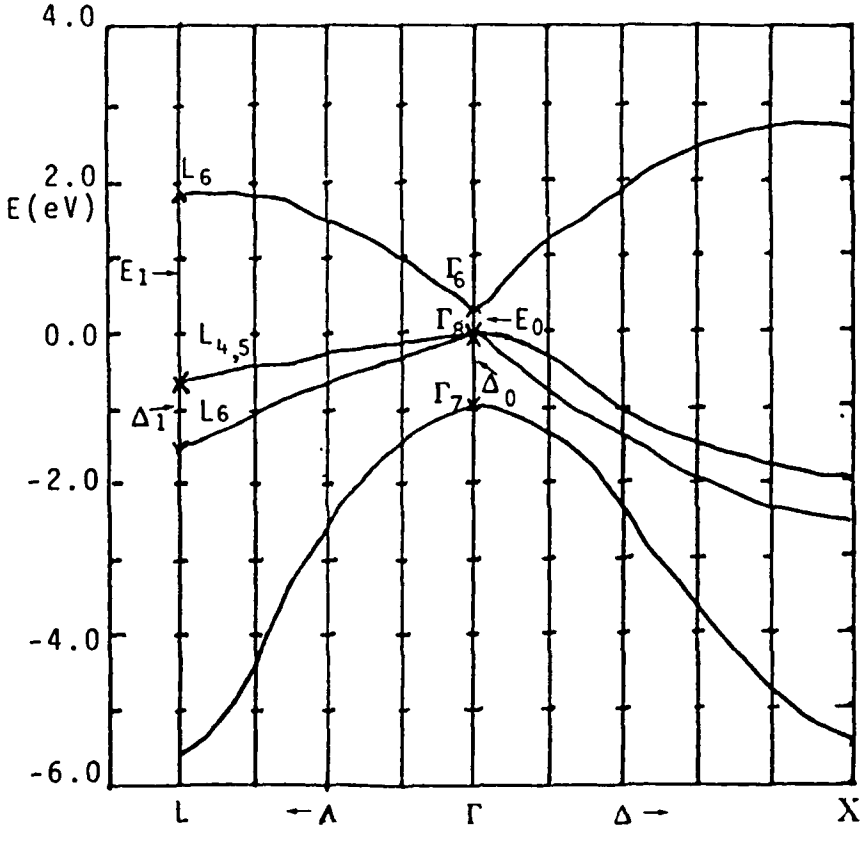

Fig. 12

Chapter VIII

GENERALIZED THEORY OF MODULATION SPECTROSCOPY BY EER & ASE

8.1 INTRODUCTION

Electrolyte electroreflectance has been used very extensively to determine accurately the interband transition energies of compound semiconductors and of alloys (Rowe, et al, 1970). The procedure is well established and illustrated in chapter 7 and, at least in the low-field limit and for centrosymmetric and relatively defect-free sample, the theory seems to fit the experiment. It assumes that the primary effect of the modulating electric field is to accelerate the optically excited electrons and therefore break the translation symmetry. Under this assumption the modulated part of the reflectance turns out to be proportional to the third derivative of the dielectric function.

Aspnes has proposed for this Third Derivative Lineshape an approximate fun· ional representation (TDL) which is most effective and explained already. When fit is made by a least-squares method to the data it yields the interband transition energy E_j, the broadening parameter Γ_j and the phase angle θ_j.

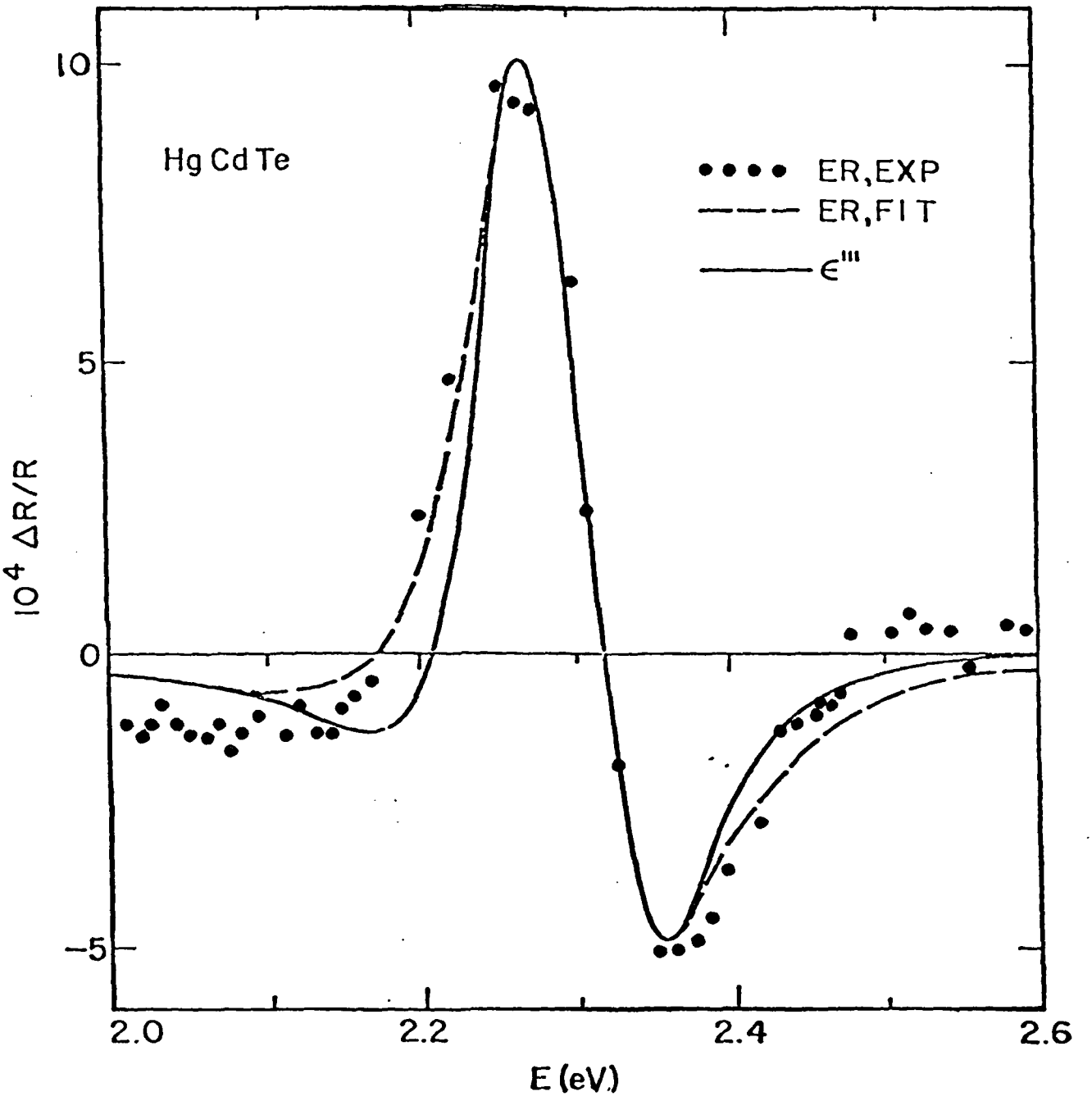

Fig. 13 Low-field EER and the best-fit, third-derivative functional form for a relatively defect-free sample of MCT, compared with the numerically calculated third-derivative spectrum from ASE for a similar MCT sample.

In the early stages of the use of EER it was considered sufficient to determine the value of the interband transition energy from the locations of the lowest energy extremum, zero crossing point and highest energy extremum in the EER lineshape (so called three-point method) (Cardona, 1969). This method is no longer credible because it has been shown repeatedly that the correct data treatment, which consists in fitting the theoretical lineshape to the experiment, yields a very different value for E_j. Having developed the necessary full lineshape analysis programs, this technique has been used extensively to determine the composition of MCT alloys as well as the variations of the composition in depth (Raccah, et al, 1983b) and laterally (Raccah, et al, 1977).

The topography of variations in composition of bulk single crystals and of epilayers as well as the profiles in composition of alloy epilayers have been most useful in the evaluation of material quality and of growth techniques. When these are used to compare materials obtained by solid state recrystallization with those obtained by the modified Bridgeman technique it turned out that the chemical inhomogenieties observed correlate very well with the electronic properties of the materials, in particular with the lifetime and mobility. On the other hand, because liquid-phase epitaxial growth (LPE) amounts to a frozen record of interfacial processes, the depth composition profiles provide essential information to the crystal growers. By using a calibrated etching procedure it was possible to make these profiles available. The results show that the epilayers are very homogeneous laterally, when compared to bulk single crystals, and that the variations in composition observed correlate very closely with the distribution of extended defects as ob-

served by STEM(Scanning Transmission Electron Microscope). This evidence for a correlation between defects and composition was further strengthened when photoemission and EER both showed that stress could modify the composition and even minority carrier type in MCT materials.

In another application the effects of surface treatment by EER have been studied. The results indicated that the MCT surface was very sensitive to chemical, electrochemical or mechanical treatments. It is observed that large variations in the EER linewidth occur with surface treatment and it is possible to correlate them with defect densities as observed by STEM or as measured by etch-pit count. These results, however, could not be confirmed by recent studies carried out by automatic spectroscopic ellisometry (ASE). A clear comparison of ASE and EER results was easy to make because, according to the theory, the very same lineshape, measured by EER, can be independently calculated by numerical differentiation from the ASE data. When comparisons of parameters obtained by EER and ASE respectively were made on a comparable sample it was found that the values of the linewidth differed by as much as 10%. The comparison is shown in Fig.(13). Moreover, they pointed out that the spectra of the real and imaginary parts ϵ_1 and ϵ_2, of the dielectric function $\epsilon(E)$, which are measured directly by ASE, are quite insensitive to chemomechanical treatment. In other words, the linewidth of the curves obtained by triple differentiation of their ellipsometric data varied very little with surface treatment whereas in our EER results it varies a great deal.

The main difference between EER and ASE is the use of a modulating electric field(for EER) as opposed to the modulation of the light polar-

ization(for ASE). It was therefore logical to infer that the discrepancy between our results and those of Aspnes et al was due at least in part to the interaction of the EER modulating electric field with the defects. In order to investigate this possibility an extensive comparative study of defectuous MCT surfaces using both EER and ASE has been carried out. These results show indeed that EER exhibits a linewidth which increases monotonically with the density of defects whereas, for the same samples, the Third-Derivative lineshape obtained from ASE data (TDA) exhibits a linewidth which hardly varies. On the other hand, the interband transition energy and therefore the alloy composition is the same when measured by either technique.

Garland and Raccah (discussed in 8.3 and 8.4) have generalized EER theory of Aspnes to take into account the effects of the interaction of the modulating $\vec{E}$ field with both extended defects and point defects and proposed a new expression for for the EER lineshape. This treatment amounts primarily to introducing, in the usual formalism, the possibilities of electrostriction and of defect polarization which are usually disregarded. Using this new expression , it has become possible to evaluate separately the relative contributions of long-range strain and of defect polarization and to understand the anomalous linewidth observed.

With the benefit of this new development a critical analysis comparing bulk single crystals to materials grown by two variants of Liquid Phase Epitaxy (LPE), Metal Organic Chemical Vapor Deposition (MOCVD) and Molecular Beam Epitaxy (MBE) has become possible.

8.2 EXPERIMENTAL EVIDENCE FOR GENERALIZED THEORY

The ASE data were taken with an ellipsometer built primarily according to the more recent design of Bermudez(1978). The samples used in the comparison of EER lineshapes to the TDA have been primarily state of the art LPE materials. A single sample can then be etched by steps as small as 500 Å and, as one proceeds from the top of the layer to the substrate, offering the opportunity to explore a wide variety of materials grown under the same experimental conditions.

In each case first the ASE spectrum and then the EER spectrum were taken. The ϵ_1 and ϵ_2 spectra were sufficiently noise-free to compute numerically the third derivatives without the benefit of noise-averaging techniques. It was therefore relatively easy to generate the third-derivative lineshape from the ASE data (TDA). It amounts to constructing a linear combination of the third derivatives of ϵ_1 and ϵ_2 using the well-known expressions for the Seraphin coefficients(1972).

These results show that for a crystal with a low defect density the TDL fits very well both the TDA and the EER spectra over a wide range of energies. In effect, the comparison in Fig.(13) shows just such a case. However, for materials with a high density of defects the situation is different in the sense that the TDL continues to fit very well the TDA but when applied to the EER spectra it meets with two difficulties well known to those who have done such work.

The first is that a constant or even a linearly varying "background" is required in order to achieve a proper fit. The second is that, even under these somewhat artificial conditions, the fit can be carried out adequately only over a narrow range of energies around E_j.

The second limitation is easy to understand because in the neighborhood of E_j the fit is not very model dependent and yields the correct critical energy in spite of a somewhat inadequate model. Consequently, the E_j's obtained from the EER and from the TDA spectra were in agreement with one another whereas the Γ_j's and θ_j's were not.

A representative example is given in Table(3), in which the values

ETCH DEPTH IN MICRONS	E_1 (eV) (E.E.R)	E_1 (eV) (A.S.E.)	x (E.E.R.)	x (A.S.E.)	Γ_1 (eV) (E.E.R.)	Γ_1 (eV) (A.S.E.)
0	2.321	2.324	.245	.249	.179	.088
1	2.355	2.354	.281	.281	.215	.087
4	2.367	2.364	.294	.291	.172	.083
7	2.377	2.374	.304	.302	.166	.084
10	2.377	2.377	.304	.304	.156	.088
13	2.383	2.384	.310	.312	.154	.092
16	2.381	2.379	.309	.306	.195	.097
19	2.384	2.385	.312	.313	.188	.090

Table 3. Values of the energy E_1, the composition x and the linewidth Γ_1 from E. E. R. and A. S. E. as a function of etch depth from a representative depth profile. The E. E. R. values were found by fitting to the third-derivative lineshape of Aspnes.

obtained for E_j and Γ_j from EER and from ASE are compared. The critical energies are in excellent agreement whereas the values of Γ_j obtained from EER are about twice those from ASE. It is this latter fact that led us to reconsider the accepted theory and to examine anew the role of the modulating electric field and its possible interaction with the defects.

8.3 GENERALIZED THEORY

Within the usual theoretical treatment of low field electroreflectance, defect scattering is not considered explicitly and the only important effect of the modulating electric field $\bar{E}$ is to accelerate the optically excited conduction electrons, giving them an added energy of the order of

$$\hbar\Omega_j = (e^2\bar{E}^2\hbar^2/8\mu_j)^{1/3}$$

where μ_j is the reduced mass in the direction of $\bar{E}$ for the jth interband transition . This assumption leads immediately to the result that the modulation $\Delta\epsilon$ in the dielectric function $\epsilon(\bar{E})$, which is caused by the field $\bar{E}$, is linearly proportional to $(\hbar\Omega_j)^3$ and to the third derivative of $\epsilon(\bar{E})$.

The results elaborated above made it necessary to explicitly treat defect scattering and to generalize the existing theory by including the small effects of the field $\bar{E}$ on defect scattering and on the interband transition energies E_j through electrostriction.

Surprisingly, it is found that shifts of as little as 0.1 meV in the E_j or in σ, which is the spatially averaged root-mean-square defect-induced variation away from the crystal potential, can substantially modify the EER lineshape. This remains true even for values of $\hbar\Omega_j$ as large as 30 or even 40 meV because the shift ΔE_j and $\Delta\sigma$ enter the theory in first order, whereas the energy shift $\hbar\Omega_j$ enters only in third order, being explicitly associated with the breaking of translational symmetry. As a result, the contribution of these shifts to $\Delta\epsilon$ scale as $\Delta E_j/\Gamma_j$, $\Delta\sigma^2/\Gamma_j^2 \equiv 2\sigma\Delta\sigma/\Gamma^2$ and $(\hbar\Omega/\Gamma_j)^3$, respectively.

The phenomenological broadening parameter Γ_j is approximately the inverse of the lifetime of the optically excited electron and is of the order of 100 meV for the E_1 and $E_1 + \Delta_1$ transitions which were studied. The shift ΔE_j gives a contribution to $\Delta\epsilon$ which is proportional to the first derivative of $\epsilon(\bar{E})$ and $\Delta\sigma^2$ gives one proprotional to the second derivative of $\epsilon(\bar{E})$.

In our generalization of the Aspnes' original theory the effect of defect scattering has been introduced exactly as he did in a later paper, following the work of Lukes and Somaratna (1970), who first introduced the quantity σ^2. Otherwise it followed exactly the original paper approach, except that the terms proportional to the small shift ΔE_j and $\Delta\sigma$ were not neglected. In particular, to obtain the generalized result the same low field expansions as Aspnes did were made

$$\Delta\epsilon_j = C_{oj}E^{-2}[(\hbar\Omega)^3 d^3/dE^3 + 6\Delta\sigma^2 d^2/dE^2 - 3\Delta E_j d/dE]E^2\epsilon(E) \qquad (68)$$

for the contribution of the interband transition to $\Delta\epsilon$, where Co_j is a constant. Still following the original treatment and making a parabolic band approximation, it is found that for the three-dimensional critical points E_1 and $E_1 + \Delta_1$, the Generalized EER Lineshape (GEL) is

$$L(E) = C_j[(\hbar\Omega_j)^3 L(E,5/2) - 4\Delta\sigma^2 L(E,3/2) - 4\Delta E_j L(E,1/2)], \qquad (69)$$

where

$$L(E,n/2) = \cos(\theta_j - n\phi_j/2)/[(E - E_j)^2 + \Gamma_j^2]^{n/4} \equiv L_n,$$

with

$$\phi_j = \mathrm{Tan}^{-1}[\Gamma_j/(E - E_j)].$$

Here, C_j and θ_j have a weak dependence on energy, which is easily taken into account by introducing the Seraphin coefficients. That energy dependence is, however, usually ignored because the evaluation of the Seraphin coefficients requires an independent knowledge of the real and imaginary parts of the dielectric function and because neglecting it only affects the determination of the parameter θ_j leaving E_j and Γ_j essentially unaffected.

It is apparent that the GEL reduces to the conventional TDL upon setting ΔE_j and $\Delta\sigma^2$ equal to zero, with L_s being proportional to the TDL. For $n = 1$ and $n = 3$, L_n is proportional to the first and second derivatives, respectively, of the same linear combination of ϵ_1 and ϵ_2

as occur in the TDL. It is clear that L_3 and L_1 have qualitatively different shapes from the TDL and from one another.

8.4 DISCUSSION

The new lineshape expression has been applied to more than 100 spectra and compared in each case to the TDL. In all cases the parameters for both interband transitions have been refined simultaneously and the GEL fits carried out over the entire experimental energy range. The results have been very consistent and the TDL, even with the additional ad hoc "background", could rarely be fit to the data over the entire experimental range. This is because an inadequate expression can only be used in the immediate vicinity of one E_j as explained above. The less defectuous materials, however, offered more favorable cases and it was sometimes possible to perform a fit over the entire energy range, thus permitting a very fair comparison with the GEL. Such a case is shown in Fig.(14).

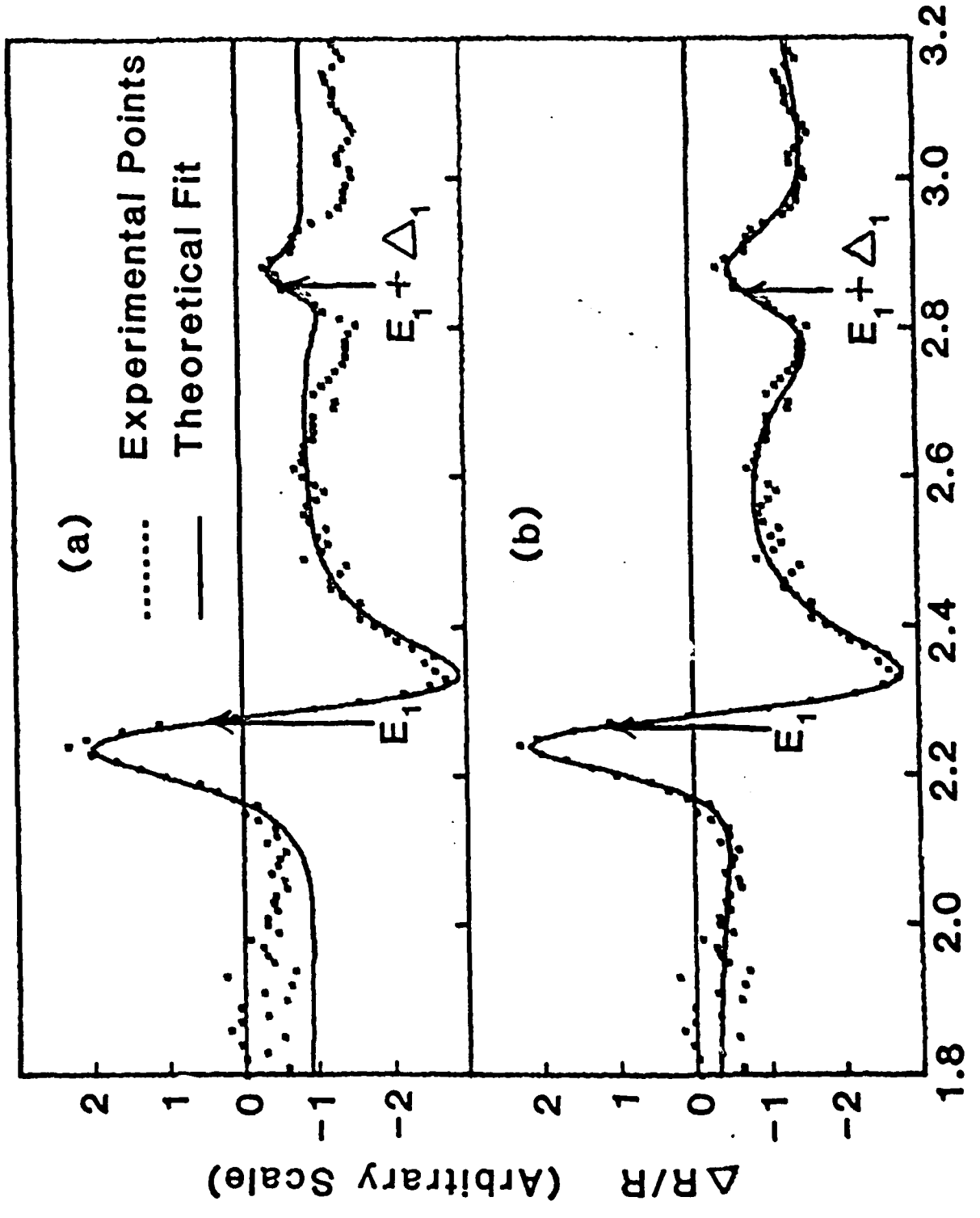
(a)
Experimental Points
Theoretical Fit
E_1
$E_1+\Delta_1$
(b)
E_1
$E_1+\Delta_1$
2
1
0
−1
−2
1.8
2.0
2.2
2.4
2.6
2.8
3.0
3.2
E (eV)
ΔR/R (Arbitrary Scale)

Fig. 14

Fig.(14a) shows that of the TDL fit while Fig.(14b) shows that of the GEL fit. It is quite clear that the TDL fit is much poorer than the GEL. Not only is the GEL lineshape phenomenologically superior to the TDL but it is also physically more meaningful. This treatment is identical to the original treatment of Aspnes' except that terms which could not legitimately be neglected in the case of defectuous semiconductor were kept. Moreover, it has already been pointed out by Rehn(1970) that in materials without inversion symmetry, as is the case here, the piezoelectric effect does cause an additional signal to be added to the regular EER spectra. He was able to separate out that signal and found it to have the proper polarization behavior. It can be said here that the GEL fits that signal well.

Consistently, it is found that in regions where high strain was expected, for example near the substrate epilayer interface, the ΔE_i term became large. On the other hand, in samples for which were known, from SIMS and transport data, that there was a high level of polarizable impurities, the $\Delta\sigma^2$ became large. The interpretation is therefore rather straightforward, and it was possible to separate out the effects of plasticity and long-range strains, which contribute strongly to ΔE_j, from the density of polarizable defects, which contribute primarily to $\Delta\sigma^2$.

Using the GEL it has been possible to study not only the compositional uniformity of materials, as was done already with the TDL, but also the nature and density of their defects. The results obtained on more than 100 samples are summarized in Table(4). In it comparison of materials grown by different techniques to state of the art bulk single

crystals was made. The techniques are LPE using regular CdTe substrate or Zn-doped CdTe substrate, Metal Organic Chemical Vapor Deposition (MOCVD) and Molecular Beam Epitaxy (MBE). The parameters compared are the sharpness S of the substrate/epilayer interface, as measured by the extent in microns of the compositional variation at the interface, the linewidth Γ_1, the Stark shift ΔE_1, the density of polarizable defects $\Delta\sigma^2$ and the growth temperatures.

It is clear that, for all types of epilayers, the quality of the material improves greatly when the growth temperature is lowered. The most spectacular results are obtained for the MBE materials which are barely distinguishable from the bulk. No less remarkable are the MOCVD materials which have come to a comparable level of quality.

EXTENT OF THE INTERFACE REGION

	[S]	GROWTH T	[ΔE_1]	[$\Delta\sigma^2$]	[Γ_1]
L.P.E. [Reg. Subs.]	3	600°C	32.5	17	115
L.P.E. [(Cd,Zn)Te]	1	600°C	20	7.5	105
M.O.C.V.D.	0.1	400°C	10	3.0	92
M.B.E.	10^{-3}	200°C	3	0.5	87
BULK			3	1.0	84

Table 4 Comparison of epilayers grown by different techniques to bulk single crystals. The parameter S is the sharpness of the epilayer/substrate interface and is stated in microns. The three defects-related parameters ΔE_1, $\Delta\sigma^2$, and Γ are stated in meV. The growth temperature of the epilayers correlates clearly with the magnitude of S and of the defect-related parameters.

Chapter IX

MIGRATION OF HG IN MCT BY STRESS

9.1 INTRODUCTION

The treatment of $Hg_{1-x}Cd_xTe$ (MCT) surfaces is delicate because of the intrinsic fragility of the material itself. By coupling photoemission with EER studies it is possible to analyze the response of MCT to mechanical shock, and conclude that under the stress, mercury tends to migrate, at least in part, via charged defects conferring an n character to the material.

In the photoemission experiments, the surface Fermi level position was measured for <110> faces of MCT prepared by cleaving in vacuum. In addition, the composition of the surface region was monitored for extended periods after cleaving for comparison to surfaces prepared in vacuum in another way. A cleavage surface was investigated by EER for both the cleavage face and the side of the crystal, which had been prepared by cutting, mechanical polishing and etching prior to cleaving. The objective in comparing the cleaved and polished surface as well as the vacuum prepared surfaces is to begin to gain insight into the critical problem of "damage" in MCT and its surface. Such knowledge is essential to economic utilization of the unique properties of MCT in infrared imaging and other possible electronic system.

Three sets of EER expriments on the E_1 interband transition of a cleaved MCT crystal have been conducted. It has been known that the EER line shape L(E) can be represented by the expression

$$L(E) = \mathrm{Re}[Ce^{i\theta}(E - E_g + i\Gamma)^{-n}, \qquad (70)$$

where the magnitude C and the phase θ are parameters which vary very little with the incident light energy E and are usually considered constant in the fit of EER line shapes.

The interband transition energy E_g and broadening parameter are the two other parameters to fit. The exponent n is determined by the symmetry of the critical point in the Brillouin zone. The exponent fitting best for all MCT results was found to be n = 2.5 which corresponds to a tridimensional point. This is expected for the E_1 interband transition in most II-VI and III-V semiconductors.

The first set of experiments was carried out on a cleaved surface (~4 x 4 mm). Many spectra were taken at various points on the surface with a well focused beam and the lineshape was fully analyzed. The results were very consistent, indicating a good uniformity of properties for the overall sample. The average values of the parameters are given, in the first line of the Table(5), with their standard deviations. The alloy composition x was determined using the relationship E_1 vs x which was established.

The second set of expriments was carried out exactly in the same manner and within the same area. The only difference was the removal of ~ 2 μ of material by the etching. The purpose of etch was to remove the cleavage damage. After anodization, carried out so as to form an oxide layer ~ 150 Å thick, the results were very consistent. They are listed in the second line of Table(5) with their standard deviations.

Finally, since the sample was essentially a cube 4 x 4 x 4 mm it was possible to carry out a third set of experiments on a side face of the sample which had been normally prepared by cutting, polishing and etching. Here this surface is used to check the uniformity in depth as well as laterally through repeated jet-etching/anodization steps of the type used to remove the cleavage damage. Again, the results were very consistent and are summarized in the third line of Table (5).

TABLE 5

Summary of results obtained by fitting the EER lineshapes in three cases. First in the case of the cleaved < 110 > face before damage removal, second in the case of the cleaved < 110 > face after damage removal and third in the case of a polished side surface of the same sample.

Results	θ	E_1 in eV	x	Γ in eV	Type
Before damage removal	0.5±0.2	2.314±.004	.220±.004	.111±0.005	n
After damage removal	0.2±0.2	2.289±.004	.188±.004	.084±0.005	p
From the polished side surface	2.2±0.2	2.284±.004	.181±.004	.167±0.005	p,n

Representative runs from the first two sets of experiments are shown in Fig.(15). As can be seen, the lineshapes are inverted one with respect to the other. Since it has already been derived that, in the low field limit, the EER signal is given by

$$\Delta R/R = qNV_m L(E), \tag{71}$$

where q is the sign of the minority carriers, N the carrier concentration, V_m the modulation voltage and L(E) the EER lineshape. This result clearly shows that the surface of the cleavage fracture inverted and has an n character consistent with the photoemission results.

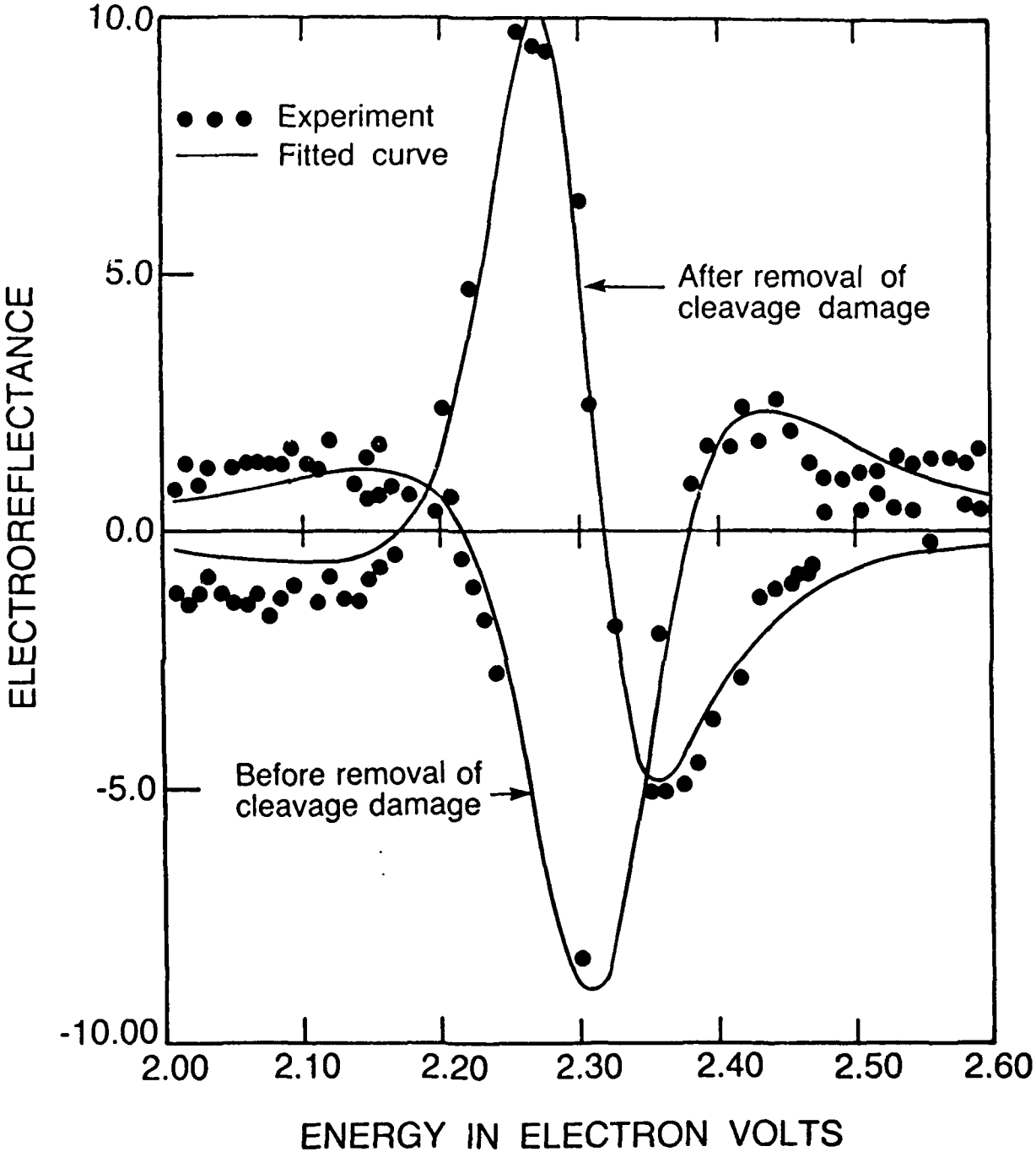

Fig. 15 EER data and fitted lineshape. The lineshapes are clearly inverted with respect to one another.

As can be seen in Table (5) the surface inversion observed after cleavage is associated with a high x value (~ .22) when compared with the value measured after removal of the cleavage damage (~ .188) or on the side surface, whether jet-etched or not (~ .181). The difference is well outside experimental error and indicates mercury impoverishment of the stressed volume. It is probable that mercury has actually migrated under the stress and diffused out of the surface. These results suggest that mercury diffusion occurs, at least partially, via charged defects conferring an n character to the material.

9.2 BROADENING PARAMETER

The broadening parameter Γ is primarily affected by lattice defects such as disorder, vacancies, dislocation etc. and with a soft material like MCT reflects very sensitively the response of the surface to treatment. A surface developed by cleavage exhibits a value of $\Gamma \sim$ .111 eV while a surface developed by cutting, polishing, and etching still exhibits treatment damage as shown by the large value ot $\Gamma \sim$ .167 eV. After removal of the cleavage damage Γ is order of .084eV a value not too different from that determined for defect-free GaAs surface ($\Gamma \sim$ .060eV).

Repeated jet-etching/anodization steps of the side surface to a depth of ~ 17 μ (third set of experiments) however, failed to remove entirely the damage generated by the chemomechanical polish and while there was some decrease of Γ its value (~ .142 eV) remained much higher than 0.084eV. In other words, conventional surface preparation of MCT seems to generate very deep damage which clearly affects electronic properties and is not easily removed.

Another interesting feature of the third set of experiment is the value of θ. The phase angle θ is a quantity related primarily to the strength of the electron-hole interaction and to the order of the critical point in the Brillouin zone contributing to the interband transition. The value of θ yielded by the results obtained on the conventionally prepared side surface is $\theta \sim 2.2$; this value is quite consistent with the results obtained with multitude of samples of different origins similarly prepared. However, it is very different from the value of .2 obtained from the cleaved surface.

9.3 DISCUSSION

The effects of cleavage in UHV is especially noteworthy. The region within 2 μ or less of the surface is transformed to n type and has a higher Cd content when compared with the polished surface. The "pulsed" mechanical shock of the cleave results in electrically active defect (possibly Hg interstitials) and may produce a loss of Hg from the surface region. Relaxation of the lattice following the momentary cleavage shock is sufficient to yield a high degree of perfection, as indicated by the low value of Γ and lack of subsequent Hg out diffusion. The region 2 μ below the surface is surprisingly perfect (Γ = .084 $\pm$ 0.005 eV) and has a higher a Hg content.

In contrast to the cleaved surfaces are those produced by polishing the same crystal. Here, no uniform type conversion takes place and a larger Hg content is observed in near surface region of the cleaved crystal. Rather, the θ value suggests that both n and p regions coexist with different defect densities. Thus, there may be a large degree of

local damage and nonuniformity. This is also reflected by the large value of Γ(0.167 eV). It is important to note the linewidth is still larger (0.142 eV) after 17 μ of MCT has been etched away.

Chapter X

SUMMARY

For characterization of semiconductors we can discuss two categories. One is the uniformity of alloys inwardly as well as laterally. The other aspect is the nature of defects which are not desirable but cannot be avoided in the crystal growth processes. In the latter case we want to know that what kinds of defects and how many of them are present in the semiconductors.

Therefore my first job was to get best values of constants in Eq.(67) so that better values of composition of alloys can be obtained. The task was accomplished by using end members of MCT and x = .5 MCT to calibrate a, b, c for many samples and developing full lineshape fitting for better E_1 values to boost reliability.

After using the established characterization procedures we can determine the qualities of bulk and LPE MCT samples(discussed in chapter 7 in detail). So we can tell which growth techniques, which growth conditions, which substrate polishing techniques are best to make good quality MCT alloys.

Second task was to probe defects by analyzing Γ values which indicate quantities of defects. A systematic study of lineshapes obtained by EER and by ASE on samples of MCT with varying densities of defects has been carried out. The results show that the two techniques yield in all cas-

es the same values for interband transition energies E_j. Since the values of the E_j are quantitatively related to the alloy composition x, it is clear that both EER and ASE can be used to carry out studies of the alloy composition.

On the other hand the values of the linewidths Γ_j yielded by the two techniques often do not agree. In those cases in which the etch pit density is less than $10^6/cm^2$, the values agree approximately; otherwise, EER yields much larger values. The difference between the two techniques is, of course, the use of an electric field modulated at very low frequencies (in EER). It was shown that the modulating electric field causes an electrostriction and polarization of the defects in MCT. These effects, which have not been taken into account in previous theories of electroreflectance, are shown to give rise to first- and second-derivative lineshapes proportional to Stark shifts ΔE_j and to a shift $\Delta\sigma^2$ related to the overall defect scattering strength, repectively. These new lineshapes dominate the usual third-derivative lineshape for defective materials.

A simple interpretation of the experimental results suggests that the relative Stark shifts ΔE_j are associated with plasticity, long-range strains and extended defects, and that the shift $\Delta\sigma^2$ arises from polarizable charged defects. All of these new values are used to enlarge the comparison of growth techniques. These results indicate that those techniques with lowest growth temperatures yield the best materials.

Using new parameters introduced in a modified theory we can tell the relative size of different kinds of defects but still cannot tell the

absolute size of each category of defects. More work is necessary for this goal.

LIST OF REFERENCES

Aspnes, D. E., and Bottka, N., Semiconductors and Semimetals, vol. 9 (Modulation Techniques). New York and London: Academic Press, 1972a.

Aspnes, D. E., Surface Science. Amsterdam, New York, Oxford, Tokyo: North-Holland Publishing Co., 1973.

Aspnes, D. E., Physical Review, B vol. 10, number 10. New York: American Institute of Physics, Nov., 1974.

Aspnes, D. E., Physical Review Letters, vol. 28, number 14. New York: American Physical Society, April, 1972.

Aspnes, D. E., Handbook on Semiconductors, vol. 2 (Modulation Spectroscopy). Amsterdam, New York, Oxford: North-Holland Publishing Co., 1980.

Aspnes, D. E., Handler, P., and Blossey, D. F., Phys. Rev., 166, 921. New York: American Institute of Physics, 1968.

Aspnes, D. E., and Rowe, J. E., Solid State Commun., 8, 1145. New York: Pergamon Press, 1970.

Aspnes, D. E., and Rowe, J. E., Phys. Rev., B5, 4022. New York: American Institute of Physics, 1972b.

Bermudez, V. M., and Ritz, V. H., Applied Optics, 17, 542. New York: American Institute of Physics, 1978.

Callaway, J., Phys. Rev., 130, 549. New York: American Institute of Physics, 1963.

Callaway, J., Phys. Rev., 134, A998. New York: American Institute of Physics, 1964.

Cardona, Manuel., Solid State Physics (Modulation Spectroscopy). New York and London: Academic Press, 1969.

Casula, F., and Kisiel, A., Nuovo Cimento, 393, 470. Bologna: Europhysics Journal, 1977.

Epifanov, G. I., Solid State Physics. Moscow: Mir Publishers, 1979.

Greenway, David L., and Harbeke, Günter., Optical Properties and Band Structure of Semiconductors. New York: Pergamon Press, 1968.

Keldysh, L. V., Sov. Phys. - JETP, 7, 788. New York: American Institute of Physics, 1958.

Kisiel, A., Acta. Phys. Polon., A39, 245. Warsaw-Cracow: Polish Academy of Science, 1971.

Kittel, Charles, Introduction to Solid State Physics Fifth Edition. New York: John Wiley, 1976.

Luke, T., and Somaratna, K. T. S., J. Phys., C: Solid State Phys., 3, 2044. Bristol: The Institute of Physics, 1970.

Magee, T. J., Proc. Sixth Conf. Crystal Growth/AACG, Fallen Leaf Lake, California. 1982.

Moritani, A., Tanigichi, K., Hamaguchi, C., and Nakai, J., J. Phys. Soc. Jpn., 34, 79. Tokyo: Physical Society of Japan, 1973.

Podgorny, M., and Czyzyk, M. T., Solid State Commun., 32, 413. New York: Pergamon Press, 1979.

Raccah, P. M., Lastras-Martinez, A., Lee, U., and Zehnder, J., J. Vac. Sci. Technol., vol. 21, number 1. New York: American Vacuum Society, May-June, 1982.

Raccah, P. M., Lee, U., Silberman, J. A., Spicer, W. E., and Wilson, J. A., Applied Phys. Lett., vol. 42, number 4. New York: American Institute of Physics, 1983a.

Raccah, P. M., and Lee, U., J. Vac. Sci. Technol. A, vol. 3, no. 1. New York: American Vacuum Society, July-Sept, 1983b.

Raccah, P. M., Garland, J. W., Zhang, Z., Lee, U., Xue, D. Z., Abels, L. L., Ugur, S., and Wilinsky, W., Physical Review Letters, vol. 53, No. 20. New York: The American Physical Soiety, Nov., 1984.

Raccah, P. M., Lee, U., Ugur, S., Xue, D. Z., Abels, L. L., and Garland, J. W., J. Vac. Sci. Technol. A, vol. 3, No. 1. New York: American Vacuum Society, Jan-Feb, 1985.

Rehn, V., Solid State Commun., 8, 1437. New York: Pergamon Press, 1970.

Rowe, J. E., and Aspnes D. E., Phys. Rev. Lett., 25, 162. New York: American Institute of Physics, 1970.

Seraphin, B. O., Proceedings of the international conference on the physics of semiconductors. Paris: Dunod Cie, 1964.

Seraphin, B. O., and Bottka, N., Semiconductors and Semimetals, vol. 9 (Modulation Techniques). New York and London: Academic Press, 1972.

Seraphin, B. O., and Bottka, N., Physical Review, vol. 145, number 2, 628. New york: American Institute of Physics, May, 1966.

Seraphin, B. O., in Optical Properties of Solids, edited by Abelès, p163. Amsterdam: North-Holland, 1972.

Spicer, W. E., Silberman, J. A., Raccah, P. M., Lee, U., and Wilson, J. A., Applied Physics Letters, 42(4), 374-376. New York: American Institute of Physics, 1983.

Tharmalingam, K., Phys. Rev., 130, 2204. New York: American Institute of Physics, 1963.

Van Vechten, J. A., and Bergstresser, T. K., Phys. Rev. B1, 3351. New York: American Institute of Physics, 1970.

Wooten, Frederick, Optical Properties of Solids. New York and London: Academic Press, 1972.

VITA

Unchul Lee was [redacted] He attended Hamyol Elementary School in Iksan-gun from 1951 to 1957, Hamyol Junior High School in Iksan-gun from 1957 to 1960. He left hometown to attend Chonju Normal School in Chonju city from 1960 to 1963 and taught Seoul Elementary School next two years.

Then he entered Seoul National University to study physics on March, 1965 after quitting teacher position and graduated from S.N.U. in 1972 with B.S. Also he served Korean Army from 1965 to 1968 , which interupted his study. He had worked for Joong-Ang Daily News (newspaper) three years as a science reporter. After that he came to U.S.A. in 1975 to Indiana University and transferred to University of Illinois at Chicago in 1977.

He got M.S. in 1981 and Ph. D. in 1985. While a graduate student at the University of Illinois at Chicago he held a teaching assistantship and later on research assistantship. As a result of research made in last three and half years, six publications and this thesis were produced. He is a member of the American Physical Society.

Publications:

"Electrolyte Electroreflectance Study of the Effects of Anodization and of Chemomechanical Polish on $Hg_{1-x}Cd_x$ Te," with A. Lastras-Martinez, J. Zehnder and P. M. Raccah, Journal of Vacuum Science and Technology, 21(1): 157-160, (1982).

"Comparative Studies of Mercury Cadmium Telluride Sigle Crystal and Epitaxial," with P. M. Raccah, Journal of Vacuum Science and Technology, A1(3): 1587-1592, (1983).

"Evidence of Stress-Mediated $Hg_{1-x}Cd_xTe$," with P. M. Raccah, J. A. Silberman, W. E. Spicer and J. A. Wilson, Applied Physics Letters, 42(4): 374-376, (1983).

"Comparative Study of Defects in Semiconductors by Electrolyte Electroreflectance and Spectroscopic Ellipsometry," with P. M. Raccah, J. W. Garland, Z. Zhang, D. Z. Xue, L. L. Abels, S. Ugur and W. Wilinsky, Physical Review Letters, Vol. 53, 1958 (1984).

"Study of Mercury Cadmium Telluride (MCT) Surfaces by Automatic Spectroscopic Ellipsometry (ASE) and by Electrolyte Electroreflectance (EER)," with P. M. Raccah, S. Ugur, D. Z. Xue, L. L. Abels, and J. W. Garland, Journal of Vacuum Science and Technology, A 3(1), 138, Jan./Feb. (1985).

"Study of Mercury Cadmium Telluride Epilayers Grown by Metalorgan Vapor-Phase Epitaxy," with P. M. Raccah, J. W.

Garland, Z. Zhang, S. Ugur, S. Mioc, S. K. Ghandi and I. Bhat, Journal of Applied Physics, 57 (6) 2014 (1985).